Final Technical Report External Grant Award Numbers:
04HQGR0087, 04HQGR0086

ANOMALOUS EM SIGNALS AND CHANGES IN ELECTRICAL RESISTIVITY AT PARKFIELD: COLLABORATIVE RESEARCH BETWEEN THE UNIVERSITIES OF CALIFORNIA AT BERKELEY AND RIVERSIDE AND OREGONSTATE UNIVERSITY

H. Frank Morrison; Lawrence Berkeley Laboratory, 1 Cyclotron Road, Mail Stop 90R1116; Berkeley CA 94720; Telephone: 510-642-3157; Fax: 510-642-3805; Email: hfmorrison@lbl.gov;

Karl N. Kappler; Berkeley Seismological Laboratory, 215 McConeHall, University of California; Berkeley CA 94720; Telephone: 510-643-3898; Email : kappler@newton.berkeley.edu;

Gary D. Egbert; College of Oceanic and Atmospheric Sciences; Ocean Admin Bldg 104; Oregon State University; Corvallis OR, 97331-5503 Telephone: 541-737-2947; Fax:541-737-2064; Email: egbert@coas.oregonstate.edu;

Abstract

Fluctuations of resistivity and anomalous electromagnetic (EM) signals have often been reported as precursors to earthquakes. Most of these reports are based on anecdotal observations of unusual phenomena associated with distant earthquakes and the signals are often orders of magnitude larger than those predicted from laboratory measurements and expected stress and strain changes, leading to considerable uncertainty as to their reliability. In an attempt to assess the validity of these reports and to understand how such signals might be generated, we have been monitoring resistivity changes and EM signals at Parkfield, the site of a focused earthquake prediction experiment. Active data collection extended for more than a year on either side of the long anticipated Parkfield Mw=6.0 event of 28 September 2004. In this progress report we discuss signal processing of these long-term data, and show some preliminary results. The long-term analysis sets out to determine whether or not statistically significant 'anomalous' signals are associated with the local Parkfield event. A variety of trends are revealed by our monitoring, but at present we have not made any observations which can be directly related to fine-time scale tectonics.

NON-TECHNICAL ABSTRACT

There are many reports of anomalous electric and magnetic fields at frequencies from quasi-DC to several 10's of Hertz, and changes in ground resistivity, prior to earthquakes. Most reports are devoted to one or another of these phenomena using a variety of measurement configurations and data processing techniques. It is the objective of this study to determine whether significant changes in resistivity, quasi-DC electrical fields, or Ultra-Low Frequency (ULF) electric and magnetic fields occur before earthquakes in California.

0.1 Introduction

Many investigators have suggested that observations of unusual geoelectromagnetic behavior are associated with seismic activity, e.g. *Corwin* (1977), *Fraser-Smith* (1990), *Molchanov* (1992), *Uyeda* (2000), *Varotsos* (1984), (for a more extensive list see references in *Pulinets* (2005), *Park* (1993), and *Johnston* (1998). *Geller* (2006, 1997) draws attention to a lack of consensus in the geophysical community on the validity and scientific merit of these reports. A collaboration of researchers at the University of California (Berkeley and Riverside) and Oregon State University established a network of electromagnetic observatories to engage in long term monitoring of EM fields and ground resistivity (*Morrison et. al.* (2004), *Egbert* (2005). Active data collection extended for more than a year on either side of the long anticipated Parkfield $M_w = 6.0$ event of 28 September 2004, which was located around 20km from the Parkfield EM installation. In this progress report we discuss a plan for a long-term analysis of these data, and show some prelimanary results. The long-term analysis sets out to determine whether or not statistically significant 'anomalous' signals are associated with the local Parkfield event. *Hayakawa et.al.* (2001) compartmentalises the observational literature which associates anomalous EM behaviour with earthquakes into four main categories: 1) Quasi-steady fields, 2) Alternating EM fields, 3) Perturbations in atmosphere and ionosphere revealed from ground-based sounding, and 4) Selected methods of satellite monitoring. We point out that our results apply only to categories one and two. With the exception of long term changes in magnetic field, we perform a search for all of Hayakawas category one effects. These are coseismic magnetic field variations, Long-term electric field variations, and ground resistivity variations. We cannot monitor long period changes in magnetic field as our instruments are not designed to monitor signals with period greater than 10^4s. With regard to category two we point out that we do not perform a search for so-called seismo-electric signals (SES) *Varotsos et. al.* (2001,1984), but focus only on ULF Magnetic Emissions in the 0.01-10Hz range. A variety of long term data trends are revealed by our monitoring, but at present we have not made any observations which can be clearly interpreted as earthquake precursors.

In this report the data are presented in a number of formats. A robust multiple station MT impedance estimate, and frequency domain residual analysis as per *Egbert* (1997) and *Eisel* (2001), Pricipal Components techniques as per *Hattori* (2005), and Canonical Coherences *Egbert* (2005).

Viewing the data through these 'lenses', we believe, constitutes a duly diligent search for indicators of anomalous phenomena in the recorded fields, as well as in ground conductivity estimates derived from these fields.

We begin section two with a brief survey of prior work and observations around the times of earthquakes. We emphasize the material presented at the Lake Arrowhead Workshop in 1992, which motivated the selection of the fields which we monitor. We then describe the experiment in terms of objectives, and the extent to which these have been met. A description of the sites in terms of location, instrumentation, hardware filtering, telemetry, and archiving is included. The archived data are the "raw data" upon which the signal processing described in section three is applied. In section four the preliminary results of the processing are presented in the form of a sequence of long term data plots. Instrument noise levels and transfer functions will be depicted using standard language and techniques.

0.2 Background

The EM array which collects the data considered in this paper is capable of monitoring ULF magnetic Fields([10^{-4} - 40]Hz), and quasi-DC electric fields ([0-40]Hz). The magnetic and electric observations are generated using standard instruments (described below), and the apparent resisitivity profiles are derived from the E, H transfer functions (impedance tensor estimates) *Simpson and Bahr* (2005). The array had three key objectives: a) Provide a continuous data source from which to conduct analysis of intersite transfer functions (TFs); b) Provide continuous measurements of apparent resistivity using robust MT remote reference processing techniques *Egbert* (1986, 1997); and, c) Archive the MT data stream in a publicly accessible storage medium for the use of other researchers. The TF analysis is intended to generate plots of residual data at either site. Residuals are to be calculated at all channels for both sites using robust remote reference (RR) processing which relates the recorded fields by means of a linear intersite TF *Eisel* (2002). Residual fields above the instrument noise levels represent signals which do not satisfy the incident plane wave assumption of the MT source-field (solar wind-magnetosphere interactions, or the earth-ionosphere resonance cavity *Berdechevsky* (2002)), as these sorts of fields would be detected at both sites *Egbert* (1989, The Source Field). To our knowledge, no long term monitoring of EM RR residuals along a fault zone have been

published to date. Long term monitoring of apparent resisitvity has been done passively in the past *Eisel* (2002), and using controlled source resisvity mapping (current injection) *Zhao et. al.* We employ similar signal processing and analysis to that of *Eisel* (2001). The archiving of the data allows the sites to act as RR for other researchers, and to validate the background fields they may observe. Besides these primary purposes a host of other measurements and indices can be derived from the long period time series, such as MA indices *Bernardi* (1989), principal components *Egbert* (2000), and canonical coherences *Brillinger* (1975), *Lyubushin* (1998). Finally, the archiving allows observed field amplitudes to be easily cross validated against Kp Indices and other auxillary datasets. The public availibility of the data enable any interesed researchers to perform their own experiments and signal processing with the array data. Both of the monitored fields have a wavelength in free space considerably larger than the earth's radius, satisfy the critereia of quasi-stationarity *Berdechevsky* (2002), and are appropriate for MT analysis techniques. We focus our analysis in this paper only on the Sept 28 2004 Parkfield Earthquake (M6). Previous research has suggested that an EQ needs to be al least ML 5.5 in order to provide a detectable magnetic anomaly *Fenoglio* (1993), whereas *Ma* (2004) argues (unconvincingly) that geoelectric disturbances can be seen preceeding M3.8, 4.1.

0.2.1 Observed Phenomenon

In the ULF band, anomalous magnetic signals were detected prior to the 1989 Mw=7.1 Loma Prieta (LP) earthquake *Fraser-Smith* (1990). These signals were characterized by increased power spectral density about one month prior to LP, which returned to normal levels several weeks after LP. About three hours before LP an outlier spike was observed in the data. Similar observations were reported prior to the 1988 Spitak (6.9) earthquake in Armenia *Molchanov* (1992). "Anomalous" behavior was seen in ULF magnetics in Japan *Kopytenko* (2002), and at least four other independent observations of magnetic field varaitions prior to earthquakes are noted in a review paper *Park et. al.* (1993). Changes in geoelectric self-potential (SP) have been reported in Japan *Uyeda* (2000) Greece *Varotsos* (1984, 1993), and the United States *Corwin* (1977). Again, at least three other observations were mentioned by *Park et. al.* (1993). These SP changes take the form of bays, or sharp offsets followed by slow decays to background levels and last on the order of minutes to hours. We note that signals having these characteristics

are ubiquitous in the Parkfield array data. Changes in resisitivty are likewise cited in the literature *Mazella* (1974), *Park* (1991), but have been criticised as having wide error bars *Morrison* (1979). A Chinese study *Zhao* (1992) consisting of 20 years of data about the 7.8 magnitude 1976 Tangshan earthquake with 0.4% error bars offers a challenge to critics, by showing a gradual 4% lowering and raising of resistivity in the shallow crust, activating slowly over a four year window centered around the earthquake.

We note that several negative results have been published for each of the above mentioned anomlous behaviours, i.e. monitoring has been done near earthquake epicenters and no changes or perturbations beyond expected values were reported around the times of earthquakes. In the ULF magnetic field these include *Karakelian et. al.* (2002), *Fraser-Smith et. al.* (1994). Much debate concerning quasi-DC electrical signal's existence, consistancy, and validity has taken place regarding so called VAN earthquake signals. Statistical validity of the VAN method has come under strong criticism in the past *Mulargia* (1992), *Wyss* (1996), *Geller* (1996). No consensus on VAN method validity appears to have been reached. Papers cite the VAN success rate any where from 50-60% *Varotsos* (1996), *Varotsos* (1993), with a 99.8% cetainty that the VAN method is more accurate than a random scheme *Hamada* (1993), to a 69-98% probability that the VAN signals are completely uncorrelated with earthquakes *Wyss* (1996), *Mulgaria* (1992), *Kagan*, (1996). The validity of the VAN method remains in question as long as until the community cannot agree. A chapter of the VAN debate is documented in *Geller* (1996, whole issue). In the case of resistivity anomalies we cite a negative results detailed in *Fitterman* (1977), *Morrison* (1979), *Park* (1991,1993).

0.2.2 Summary of Lake Arrowhead Conference

The Lake Arrowhead Conference (LAC) in 1992 was entitled: "Low Frequency Electrical Precursors: Fact or Fiction?". The consequent attitude was that there did seem to be some (a few) credible observations of ultra-low frequency magnetic field, quasi-DC electric field, and resistivity anomalies, possibly related to earthquakes. The following caveats regarding the observations were acknowledged:

a) The cited phenomena are not clear outliers against an objective statistical criterion.

b) The instrument calibrations are not made with respect to some absolute standard, and/or instrument observations are published without citing

system transfer functions and noise level analysis

c) The observation can not be shown to fit into accepted physical models, and is without plausible physical explanation.

It is our intent to nullify caveats a and b for earthquake signals. We neglect c under the principle that observation is logically prior to modeling in the absence of a theoretically predicted effect based on accepted principles. i.e.: No model is required until credible observations have been widely acknowledged.

Two practical methods of approaching a resolution to the earthquake precursor validity question arose out of the conference. Since some phenomena, such as those reported by *Fraser-Smith* (1990) and *Qian* (1992), reportedly begin before earthquakes, and continue on afterwards, this suggests a practical experiment to determine whether precursory phenomena may be occurring. Researches could deploy selected field monitoring equipment immediately after an earthquake, near the epicenter, and monitor for several months afterwards. Such experiments would require reference stations, and the PKD-SAO array has been proposed to serve this reference field monitoring purpose. This post-earthquake monitoring has already been attempted with negative result *Karakelian* (2002). The other practical method would be to engage in long term monitoring of ULF signals with sparse arrays in regions where significant seismicity is widely believed to occur repetitively.

The EM array which collects the data considered in this paper is capable of monitoring ULF magnetic Fields([10^{-4} - 40]Hz), and quasi-DC electric fields ([0-40]Hz). The magnetic and electric observations are generated using standard instruments (described below), and the apparent resistivity profiles are derived from impedance tensor estimates *Simpson and Bahr* (2005).

The key objectives of the array were to:

a) Provide a continuous data source from which to conduct analysis of inter-site transfer functions (TFs);

b) Provide continuous measurements of apparent resistivity using robust MT remote reference processing techniques *Egbert* (1986, 1997);

c) Archive the MT data stream in a publicly accessible storage medium for the use of other researchers.

These objectives were partially motivated by reports of fluctuations in apparent resistivity *Mazella* (1974), *Zhao* (1992) anomalous ULF [0.01-10]Hz magnetic fields *Molchanov et. al.* (1992), *Fraser-Smith et. al* (1990) and quasi -DC electrical fields *Corwin* (1977) *Uyeda* (2000) as occurring before, during and after large earthquakes. We focus our analysis in this paper on

the search for these sorts of phenomena about the Sept 28 2004 Parkfield Earthquake (M6).

0.3 Sites and Instrumentation

The specific locations of the sites were chosen in anticipation of the next M_w 6.0 earthquake which seems to be a repeating phenomenon on a time scale of 22 years (*Tullis* (1999)). In 1996 the array began collecting data. The locations of the sites, a distance of 150 km apart are detailed in Figure 1.

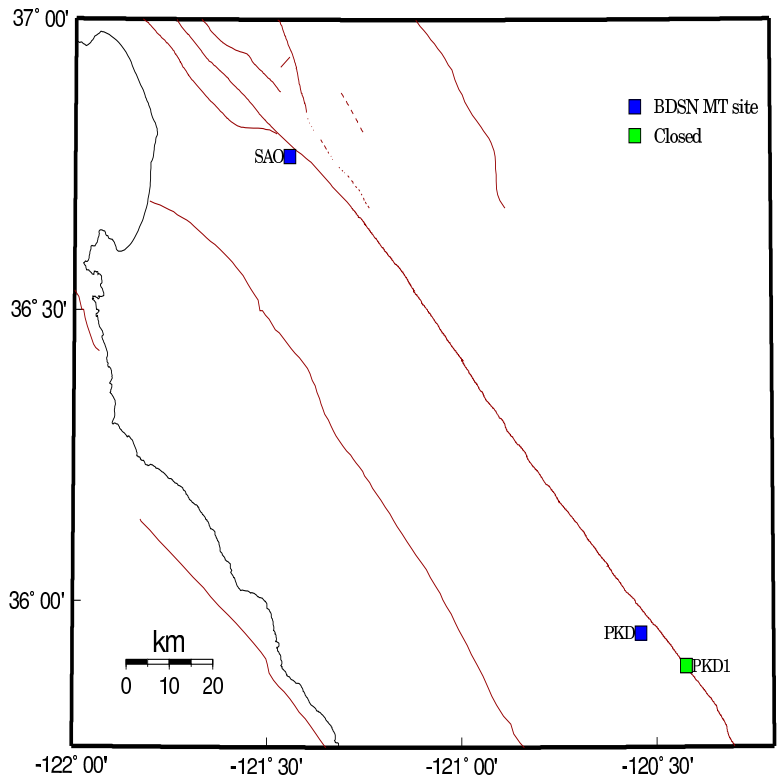

Figure 1: Map illustrating the location of operational (filled squares) and closed (grey squares) MT sites in central California.

At each observatory, three induction coils (model EMI BF-4) measure the time varying magnetic field, and two 100m long electrodes measure the electric field in the surface plane. The coils are buried in 0.5m trenches. The Electrodes are Pb-PbCl non-polarizing type, and are placed in 3m holes with moist bentonite packing to keep contact resistance to a minimum. The entire system is powered by 12V batteries with constant trickle charge provided by

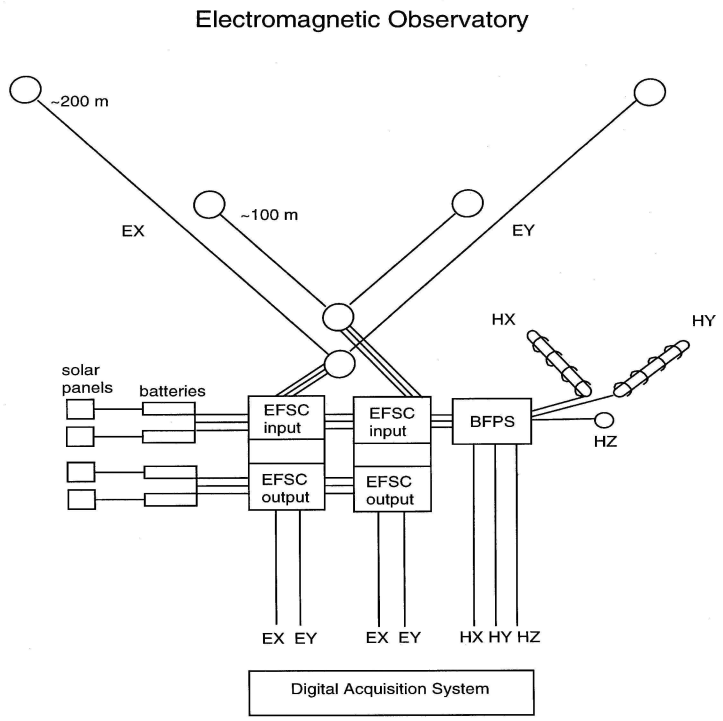

Figure 2: Schematic diagram of EM observatory with two sets of electric dipoles.

Site	Latitude	Longitude	Elev(m)	Date	Location
PKD	35.945171	-120.541603	583	1999/02/05-	Parkfield
PKD1	35.8894	-120.426109	431.6	1995/06/06 - 1999/03/08	Parkfield
SAO	36.76403	-121.447722	317.2	1995/08/15	Hollister

Table 1: Specific Site Locations and dates of operation

on site solar cells. The measurements are filtered onboard the coils for a stable response over several decades of period. The dipole data are preprocessed with an Electric Fields Signal Conditioner (EFSC). The EFSC consists of a preamplifier, optical isolator, and main amplifier in series, with an optional high pass filter. The data are then digitized by Quanterra digitizers (Q935 at PKD and Q4120 at SAO), at a sampling rate of 40Hz. Time synchronization is done via Global Positioning System (GPS). The data are then telemetered in packets to the Northern California Earthquake Data Center (NCEDC) where they are archived *(www.ncedc.org)*. A schematic diagram of the site instrumentation is provided in Figure 2. At PKD, an added pair of 200m dipoles collect data alongside the 100m pair. This is useful in recognizing when one pair is malfunctioning, checking linearity of measurements, as well as being required should one want to run VAN method analysis *Varotsos* (1991). All stages of data processing are archived, including pole-zero responses (with error estimates), instrument gains, and FIR coefficients for all applied filters. Changes in these acquisition parameters are also archived when instruments are replaced. The result of this archiving is that data collected on a given day can be examined in terms of the various stages of applied preprocessing, and plotted in either machine counts or SI units to validate quality. For the purposes of this paper 'raw' field data are the signals stored at the NCEDC after instrument-applied processing.

0.4 Signal Processing

We employ robust estimates of signal to noise ratio and apparent resistivity as per *Eisel & Egbert* (2002) on data sampled at 1Hz. We calculate remote reference (RR) residuals for these 1Hz data *Gamble* (1979). Lower order principal components are calculated similar to the analysis of *Hattori* (2005).

The 1Hz time series' are processed in the spectral domain. Each UT day of raw data (86400 points) are cut into 128-point windows, with a 32-point overlap, resulting in a time series of frequency domain complex Fourier coefficients (FCs). In order to obtain lower frequency bands the data are decimated (with anti-alias lowpass filtering) by a factor of four, and the 128-point window with 32 point overlap Fourier Transform is applied again. This decimation is applied a total of three times to obtain periods as long as 1500s. For further details on the preparation of the spectral domain time series, see *Eisel & Egbert* 2001 (EE2001), or *Egbert & Booker (1986)* (EB1986).

0.4.1 Signal to Noise (SNR)

The SNR estimation is the first step of the Fourier domain data processing. The SNR plots provide a measure of day to day variations in system noise, serving as an indicator of all-around system health. SNR estimates are developed for each channel, and each frequency band, on each day. Specifics of the method are thoroughly documented in *EB1986, Egbert* (1989); we present only the essential steps. Consider a single, arbitrary, but fixed set of {day, channel, and frequency band}. Once windowed and Fourier Transformed, the data take the form of a one-dimensional time series of Fourier coefficients of some length L. We denote this 'data time series' as d(t). d(t) is raw data and may be (is almost certainly) contaminated by outliers. Each iteration consists of three parts: noise level estimation, rescaling the data, and down-weighting of outliers. The result is a 'cleaned up' incarnation of the raw data.

Initially, a linear transfer function (G(day)) is estimated between d(t) and M(t), where M(t) is a matrix whose rows are the remote site channels, together with channels of other field type at the local site, and whose columns correspond to the FT time windows.

$$\begin{pmatrix} d_1 & d_2 & \dots & d_L \end{pmatrix} = \begin{pmatrix} G_1 & G_2 & \dots & G_N \end{pmatrix} \begin{pmatrix} m_{ch1,1} & m_{ch1,2} & \dots & m_{ch1,L} \\ m_{ch2,1} & m_{ch2,2} & \dots & m_{ch2,L} \\ \vdots & \vdots & \ddots & \vdots \\ m_{chN,1} & m_{chN,2} & \dots & m_{chN,L} \end{pmatrix} \tag{1}$$

The transfer function G relates the channels making up the rows of M to the observed vector d. G is estimated using ordinary least squares. The error in this estimate is then quantified using the error timeseries e(t),

$$e = d - GM \tag{2}$$

The amplitude of the error vector is calculated using a hybrid of the L_2 and L_1 norms, designed to reduced the influence on outliers in d(t). d is then scaled by the error variance, and observations (elements of the scaled d(t), call it $d^{(0)}$) determined to be further than some predefined (1.5) number of standard deviations from the average are classed as outliers, and multiplied by a weight factor which varies as the inverse of the outlier magnitude. The process is essentially a standard Least Squares inversion performed iteratively, with the step betwixt iterations being an inwards migration of outlier data away from pdf tails. This means that d(t) is constantly being re-estimated by a less noisy timeseries. The process of TF estimation, error variance scaling, and outlier downweighting is repeated iteratively, until the time series d(t) stabilizes. This method of cleaning the data is known as the robust multivariate errors-in-variables (RME) estimator method *Huber* (1981), *EB1986*. The local, same-field-type channels are omitted from the loss functional because all these channels are run through a common data acquisition instrument. We wish for the channel being estimated to include the acquisition instrument noise, and thus no data channel common to the instrument acquiring d(t) can be included in M, lest the TF (G) cancel this instrument noise from the error time series. The RME method yields a time series of signal to noise ratio (SNR) of the form d(t)=GM(t)+e(t) where $\|e\|_H$=1 where $\|*\|_H$ refers to the hybrid norm of *EB1986*, and GM(t) is considered the time series of 'signal'. The units of the d(t) time series can then be considered multiples of the 'noise', and so {SNR in dB}=log(norm(GM)).

0.4.2 Estimation of the MT Impedance Tensor and Apparent Resistivity

The TF analysis generates stable estimates of apparent resistivity (ρ_a) which can be used to track time and frequency (depth) dependant variations in ground conductivity.

The magnetotelluric transfer function **Z** has the following structure and relationship to measured fields E and H:

$$\begin{pmatrix} E_x \\ E_y \end{pmatrix} = \begin{pmatrix} Z_{xx} & Z_{xy} \\ Z_{yx} & Z_{yy} \end{pmatrix} \begin{pmatrix} H_x \\ H_y \end{pmatrix} \tag{3}$$

Here E and H are the locally measured fields.

Equation 3 can be shown to hold perfectly when the usual MT assumptions are in place, i.e. Incident fields are plane waves of infinite horizontal extent. In practice, we know that this assumption is not exactly true *Egbert* (1989. 2000), but is a very reasonable approximation at our site latitudes. The off-diagonal elements of the MT impedance tensor are in direct proportion tothe square root to the bulk resistivity of the ground.

$$\rho_{ij} = \frac{1}{\mu\omega}\|Z_{ij}^2\| \qquad fori \neq j \tag{4}$$

The method of transfer function calculation is pedagogically the same as the RME method used for SNR estimation described above inasmuch as its iterative outlierresistant structure. Our technique of calculating the MT impedance tensor however involves both local and remote field measurements called the Remote Reference (RR) estimate, which has been found to significantly stabilize estimates of **Z**. *Gamble* (1979). The robust RR processing was suggested in *Chave and Thompson* (1989), and is outlined clearly in *Eisel and Egbert* (2001). The minor variations account for remote reference processing, and the inclusion of only other-field-type (OFT) channels.

Using RR processing, the impedance tensor estimate is estimated iteratively by:

$$Z = (RWH)^{-1}(RWE) \tag{5}$$

The estimation process is initialized using the cleaned dataset from the SNR processing as our **E**, **H**, and **R** data, where **R** corresponds to the remote site Magnetic field data, and **W** is a weight matrix initially set to **I**. At each

step, a diagonal **W** is calculated which pulls outliers in **E**, **H**, **R** toward their expected values by a factor proportional to their errancy from a predefined number of standard deviations (as in SNR). Here, 'errors' are measured using the RME hybrid norm mentioned in previous section, which is essentially an L2 norm for residuals within 1.5 standard deviations of the residual pdf, and an L1 norm otherwise. The process effectively downweights leverage points *Chave and Thompson* (1989), and allows for outliers at the reference site. Note that careful, robust estimates for σ are also required at each iteration. These are detailed in the appendix of *EB1986*. A detailed explicit recipe for computing **W** is detailed in *EE2001*, and in *EB1986*.

0.4.3 Principal Components Analysis

The PCA approach to MT was first proposed by *Jupp* (1978), and further elaborated on in *Park and Chave* (1984), *Egbert* (1989,2001), and applied specifically to the search for anomalous EM behavior associated with earthquakes by *Hattori* (2005). To conceptualize the motivation behind PCA, consider an N-channel vector-valued timeseries (VVTS) called X(t) (N=12 in our case: 7 from PKD and 5 from SAO). Imagine that these data must be continuously transmitted to a remote receiver station, but there are only M<N channels available for transmission. Imagine also that signal processing tools such as adders and multipliers are available at both the transmitter and receiver. Clearly one would want each transmission channel to be carrying a signal which is uncorrelated with each other transmission channel. In fact, in order to guarantee a minimal error (least squares difference in the original and received signals) we wish each channel to be maximally uncorrelated with each other channel, such that the M transmitted signals correspond to the M largest components of the original N dimensional TS.

The way to do this is to perform an eigenvector decomposition of the VVTS covariance matrix (XX^T, and compose the M channels of the M largest eigenvalues. Detailed derivation of this can be found in *Brillinger* (1975), or *Hyvarinen* (2001).

We show briefly how to perform a PCA for a single day for a particular frequency. Consider the VVTS time series (X_i(t)) of SNR observations at a particular frequency, derived by the process described under SNR. The subscript i acts as an index for the windowing of the original time-domain data. Each of these time series has length L≈86400/((Decimation Level+1)*4)/128, and for each day i runs from 1 to n=86400/L. To derive a single estimate of

the covariance matrix we simply compute $X_i X_i^*$. To calculate the expectation value of the covariance matirx Σ (aka Spectral Density Matrix S) we calculate:

$$\Sigma = S = \frac{1}{n} \sum_{i=1}^{n} X_i X_i^* \tag{6}$$

The SDM is a multivariate structure of the EM data which contains information about the dimensionality of signal and coherent noise. It has been shown previously (*EB1989*) that the dimension, or number of non-zero eigenvalues of the SDM will be 2 in the absence of coherent noise. This corresponds to the case where the MT plane wave assumption holds perfectly. One may expect that if EM fields were being produced by some other process, such as Earthquake preparation crustal processes, that these signals would not be coherent with the solar wind or sferic signals, and as such would be present as a separate 'principal component'. We subject the SDM to an eigenvalue decomposition, and consider only the first four principal components, since the fifth and higher components correspond to signal levels below the system noise floor.

0.4.4 Canonical Coherences

The Canonical Coherence (CC aka Canonical Correlations) method *Hotelling* (1935) *Brillinger* (1969) has not been previously applied to EM geophysical methods, but has been applied to long term geophysical monitoring by *Lyubushin* (1998). It is a method of performing a frequency dependent measure of the coherence between two VVTS's. In PCA we approximated one VVTS by a filtered version of itself, whereas here we are approximating a VVTS by a filtered version of a different VVTS. In the case where the second VVTS equals the first, the method degenerates to PCA. A well-referenced description of the CC methods as applied to geophysical data can be found in *Lyubushin* (1998); only a very condensed version of the method is given here.

The canonical coherence method works by projecting the two VVTSs (**X,Y**) onto two m-dimensional subspaces ($\mathbf{S}_X$**,** $\mathbf{S}_Y$), defined by a two sets of m basis vectors (B_X, B_Y), where m is the dimension of the smaller VVTS. The basis vectors are found as ordered pairs ($b_{i,X}$, $b_{i,Y}$), with one basis vector from each VVTS. We present a condensed derivation of the the CC method, showing that the basis vectors have the following two properties:

1.The basis vectors of each particular VVTS are orthogonal (they are uncorrelated with one another <$b_{i,X}$,$b_{i,X}$> = 0 for i $\neq$ j).

2. Each ordered pair is chosen in such a way that the elements of the VVTS' projected onto their respective elements correleate maximally.

Consider a VVTS **Z**(t) which has dimension CxL, where C denotes the number of data channels (12 in our case), and L represents the length of the TS, or number of observations. We partition **Z** into two disjoint VVTSs, **X**, and **Y**, where dim(**X**)=m, dim(**Y**)=n, m+n=C, and without loss of generality n<m. In order to determine a pair of basis vectors which correlate maximally, we seek a set of coefficients, {p1,...pm, s1...sn}, such that the linear combination:

$$e(t) = (p_1 X_1(t) + \ldots + p_m X_m(t)) - (s_1 Y1(t) + \ldots + s_n Yn(t)) = p\mathbf{X} - s\mathbf{Y} \quad (7)$$

is minimized. Here e(t) is the 'error time series'.

If the VVTS' are mean subtracted then the correlation Γ of the vectors p**X** and s**Y** is given by:

$$\Gamma = \frac{< p\mathbf{X}, s\mathbf{Y} >}{\sqrt{< p\mathbf{X}, p\mathbf{X} >< s\mathbf{Y}, s\mathbf{Y} >}} = \frac{p\mathbf{X}\mathbf{Y}^* s^*}{(p\mathbf{X}\mathbf{X}^* p^*)(s\mathbf{Y}\mathbf{Y}^* s^*)} \quad (8)$$

Alternatively we can think of this quantity as the coherence of the time-series' since we are in spectral domain looking at a single frequency band, or as the cosine of the angle between the L dimensional vectors p**X** and s**Y**. By adopting standard covariance matrix notation (Σ_{XY}=$\mathbf{X}\mathbf{Y}^*$, we can express Equation 8 in condensed form:

$$\Gamma = \frac{p\mathbf{\Sigma_X}\mathbf{Y}s^*}{\sqrt{p\mathbf{\Sigma_{XX}}p^* s\mathbf{\Sigma_{YY}}s^*}} \quad (9)$$

Now by defining two vector-valued variables:

$$\rho = (\mathbf{\Sigma_{XX}^{1/2}})\mathbf{p}^* \quad and \quad \sigma = (\mathbf{\Sigma_{YY}^{1/2}})\mathbf{s}^* \quad (10)$$

Recalling that the covariance matrices (as long as non-singular) are Hermitian, hence positive semi-definite, that therefore have a well-defined unique square root matrix (although practically speaking the condition number of Σ can be large, and the root may be computationally difficult to determine. Substituting the variables of Equations 10 into Equation 9 yields:

$$\Gamma = \frac{\rho \mathbf{\Sigma_{XX}^{-1/2} \Sigma_{XY} \Sigma_{YY}^{-1/2}} \sigma^*}{\sqrt{(\rho\rho^*)(\sigma\sigma^*)}} \tag{11}$$

Now looking at the numerator of Equation 11 as the inner product between the two vectors a and b, defined as

$$a = \rho \mathbf{\Sigma_{XX}^{-1/2} \Sigma_{XY} \Sigma_{YY}^{-1/2} and b} = \sigma^* \tag{12}$$

and substituting Equation 12 into the following form of the Cauchy-Schwarz inequality:

$$< a, b > \leq \sqrt{< a, a >< b, b >} \tag{13}$$

we obtain the following inequality

$$\rho \mathbf{\Sigma_{XX}^{-1/2} \Sigma_{XY} \Sigma_{YY}^{-1/2}} \sigma^* \leq (\rho \mathbf{\Sigma_{XX}^{1/2} \Sigma_{XY} \Sigma_{YY} \Sigma_{YX} \Sigma_{XX}^{1/2}} \rho^*)^{\mathbf{1/2}} (\sigma\sigma*)^{\mathbf{1/2}} \tag{14}$$

Now dividing both sides of the above expression by the norms of ρ and σ, the left hand side becomes exactly the expression for Γ from 11 and we obtain:

$$\Gamma \leq \sqrt{\frac{(\rho \mathbf{\Sigma_{XX}^{1/2} \Sigma_{XY} \Sigma_{YY} \Sigma_{YX} \Sigma_{XX}^{1/2}} \rho^*)}{\rho\rho^*}} \tag{15}$$

By viewing the five-matrix product in the center of the numerator in expression 15 as a single matrix:

$$A = \mathbf{\Sigma_{XX}^{1/2} \Sigma_{XY} \Sigma_{YY} \Sigma_{YX} \Sigma_{XX}^{1/2}} \tag{16}$$

we see that the expression within the square-root on the right hand side of 15 is actually a Rayleigh quotient, having form:

$$\frac{\rho A \rho^*}{\rho\rho^*} \tag{17}$$

which obtains its maximum value when ρ is the dominant eigenvector of A (note the expression is independent of any non-zero scalar applied to ρ). Thus we have determined that Γ is bounded above by the value it attains for a specific ρ for which we have a recipe as a function of the data. In order for

Γ to realize the maximum we have derived it is sufficient that the vectors a and b of expression 13 be co-linear. This is equivalent to the condition that:

$$\sigma \quad \propto \quad \mathbf{\Sigma_{YY}\Sigma_{YX}\Sigma_{XX}^{1/2}} \tag{18}$$

We have shown that there is an upper bound for Γ, and that it is attainable as long as the matrix A in Equation 17 is non-singular. It should also be clear that the next most coherent (highest Γ) linear combination of channels, which is uncorrelated (or linearly independent of) the first linear combination will correspond to the 2nd dominant eigenvector of A. The back-substitution algebra to compute p and s directly is omitted. We simply move on to provide a formula for computing the vectors p and s.

Note that this process can be thought about in time domain, where it paralells using Weiner filtering to approximate one MVTS by another, in an iterative procedure.

The SDM (or covariance matrix) of Z(t) is in fact a matrix partitioned into the cross and power spectra of our partition series' as long as we are careful to order the rows of Z so that the channels of **X** and those of **Y** are mutually consecutive, ie.

$$\mathbf{Z(t)} = \begin{pmatrix} \mathbf{X} \\ \mathbf{Y} \end{pmatrix} \tag{19}$$

A quick and practical method for computing CCs uses the covariance matrix of the VVTS Z(t) That is:

$$\mathbf{Z(t)Z^*(t)} = \begin{pmatrix} \mathbf{\Sigma_{XX}} & \mathbf{\Sigma_{XX}} \\ \mathbf{\Sigma_{YX}} & \mathbf{\Sigma_{YY}} \end{pmatrix} \tag{20}$$

The Canonical Coherences (vectors p and s) can be found by solving the eigenvalue equations:

$$\begin{aligned} \mathbf{\Sigma_{XX}^{-1}\Sigma_{XY}\Sigma_{YY}^{-1}\Sigma_{YX}^{-1}\hat{v}_x} &= \mathbf{\Gamma^2\hat{v}_x} \\ \mathbf{\Sigma_{YY}^{-1}\Sigma_{YX}\Sigma_{XX}^{-1}\Sigma_{XY}^{-1}\hat{v}_y} &= \mathbf{\Gamma^2\hat{v}_y} \end{aligned} \tag{21}$$

Here Γ^2 is the square of the correlation coefficeient for the linear combinations from the two sets, $\hat{\mathbf{v}}_x$ and $\hat{\mathbf{v}}_y$ are the canonical coherence basis vectors. We showed above that solving for one eigenvector allows us to compute the other without a computationally expensive eigenvector decomposition.

Once we have solved for example for $\hat{\mathbf{v}}_x$ then we can determine $\hat{\mathbf{v}}_y$ according to:

$$\mathbf{v_y} \;\; \alpha \;\; \frac{\mathbf{\Sigma_{YX}}\sqrt{\hat{\mathbf{v}}\mathbf{\Sigma_{YX}}\hat{\mathbf{v}^*}}}{\mathbf{\Gamma\Sigma_{YY}}} \tag{22}$$

So by normalizing the v above, we obtain a single expression for rapid unambiguous calculation of CC coefficients.

0.4.5 Residuals Analysis

Natural, everpresent, EM noise is typically on the order of a few pT to a few nT at our frequencies of interest. In order to see any local EM phenomenon on this order or smaller we need to account for the natural, or so called 'magnetotelluric' fields. Fortunately, the natural magnetic noise observed at the two sites is very nearly identical *Kappler* (2005) and the electric fields are related by a time-invariant transfer function. The intersite transfer function (TF) is subject to some noise, but we stabilize the estimate by using a median TF which is averaged over all the 'good' days in 2004. It is important that the median TF be devoid of days of anomalously high geomagnetic activity, or at least to downweight these data. The fields at Parkfield are then estimated in various bands by using only the data at Hollister and the median TF. The residual difference between predicted and observed field is then a measure of, among other things, EM noise which is specific to Parkfield, and is not contained in the natural MT field. The residual data are still being processed at the time of this report, but a sample residual plot for Parkfield Hx data is shown below. On the same plot is a measure of global geomagnetic activity index (Ap). We see that some of the departures from typical residuals seem related to times of unusually high Ap values. We also see that the residuals in the time around the earthquake (day 272) do not depart in an obvious way from their behavior at othertimes. There is some evidence for a different residual mean value before and after the earthquake, but confirming it requires analysis of a longer time series. We are actively working on expanding the reisdual TS to include all channels at PKD, and a four-year time range.

0.5 Results

0.5.1 Signal to Noise Ratios

Signal-to-noise ratios estimated daily from the 1Hz data by RME method are shown in Figures 6 for all primary channels in the array. This plot is a "warts-and-all" view of the whole dataset. There are frequent gaps in data, delineating times where data were not collected, or where signal was clear ly corrupted by instrument malfunctions. The corrupt instrument times were identified by visual inspection. Although the number of gaps can be reduced in a more thorough analysis through the use of TFs to estimate a missing remote channel, for uniformity of signal processing on a "first-pass" of the data, we omit all channels from days where one or more channels are highly contaminated. The "hand-editted" data are displayed in Figure 5. It is cl ear that the health of the system needs to be monitored in real time so that these gaps can be reduced in long-term monitoring.

The pulse-like broadband hot-spots on day210, 2004 and day315, 2004 stand out in the time series. These seem to be magnetic storms since they correlate betwe en sites as well as with the global K_p A_p indices. We consult the A_p indices published by GFZ-Potsdam, and find that the pulses align nicely wi th the dominant spikes in the 4-year A_p plot (see Figure 7). With regards to the fields observed near the earthquake time, the EM monitoring arra y primary channels were functioning well when the Parkfield earthquake occurred.

We see a seasonal trend in the electric field data at PKD which seems to correlate with the rainfall timeseries (see Figues 9 and 10). The seasonal electric field SNR variation is negligible at SAO. This suggests that local geology is a factor in controlling the noise levels. It is possible that ions being liber ated into solution by rainfall are resulting in local chemical gradients and hence streaming potentials active at the Parkfield site. Also, ionic liberation in a heterogeneous near surface layer could be a cause for conductivity anomalies which appear and disappear over seasonal time scales.

0.5.2 Apparent Resistivity Plots

We characterize temporal variations of apparent resistivity in terms of deviation from median. Using the robust outlier cleanup method with a window length of 40, and overlap of 15, threshold set at 1.0 standard deviations and

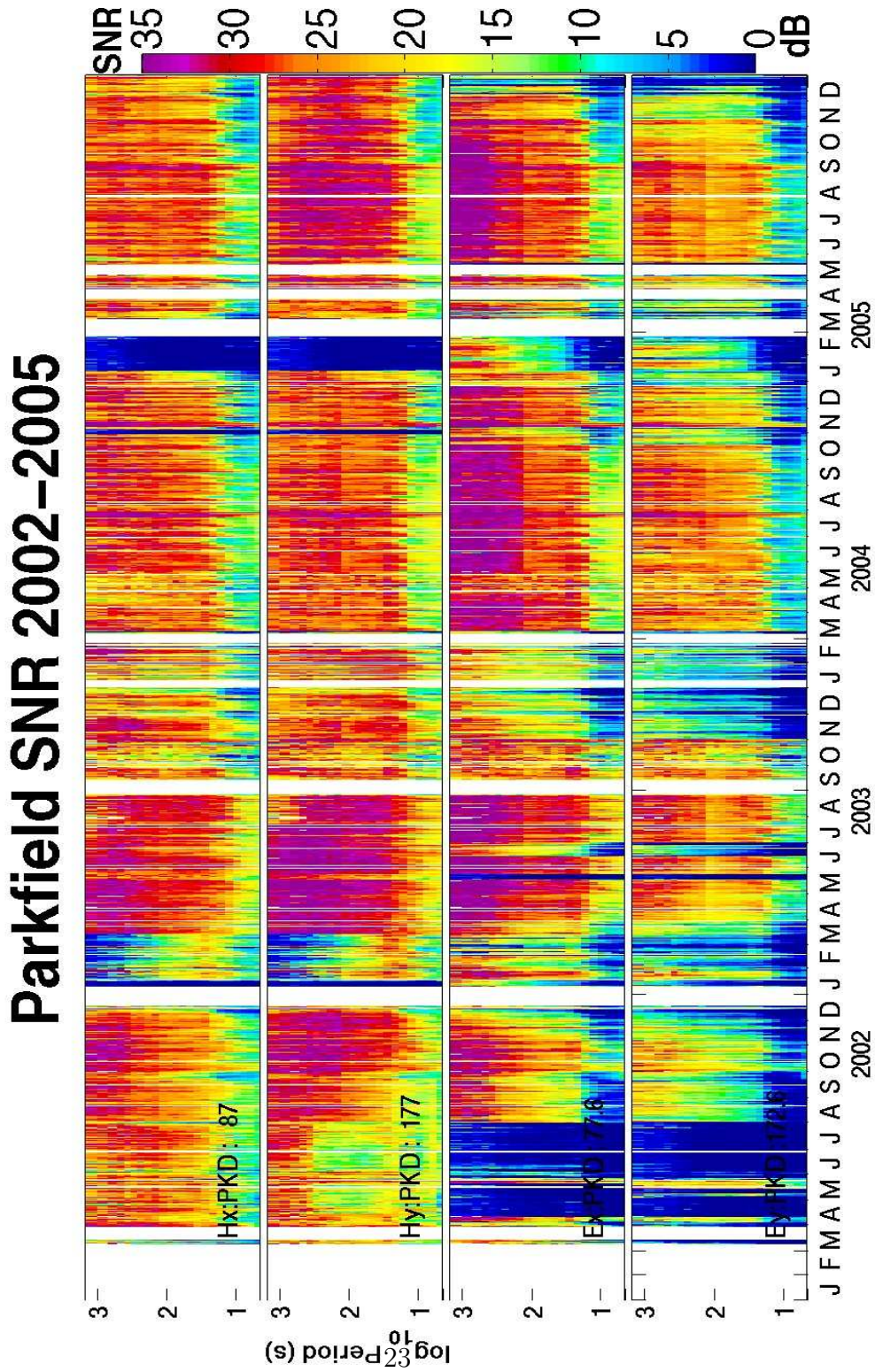

Figure 3: Parkfield Electric and Magnetic Field SNRs for four years, including contaminated data

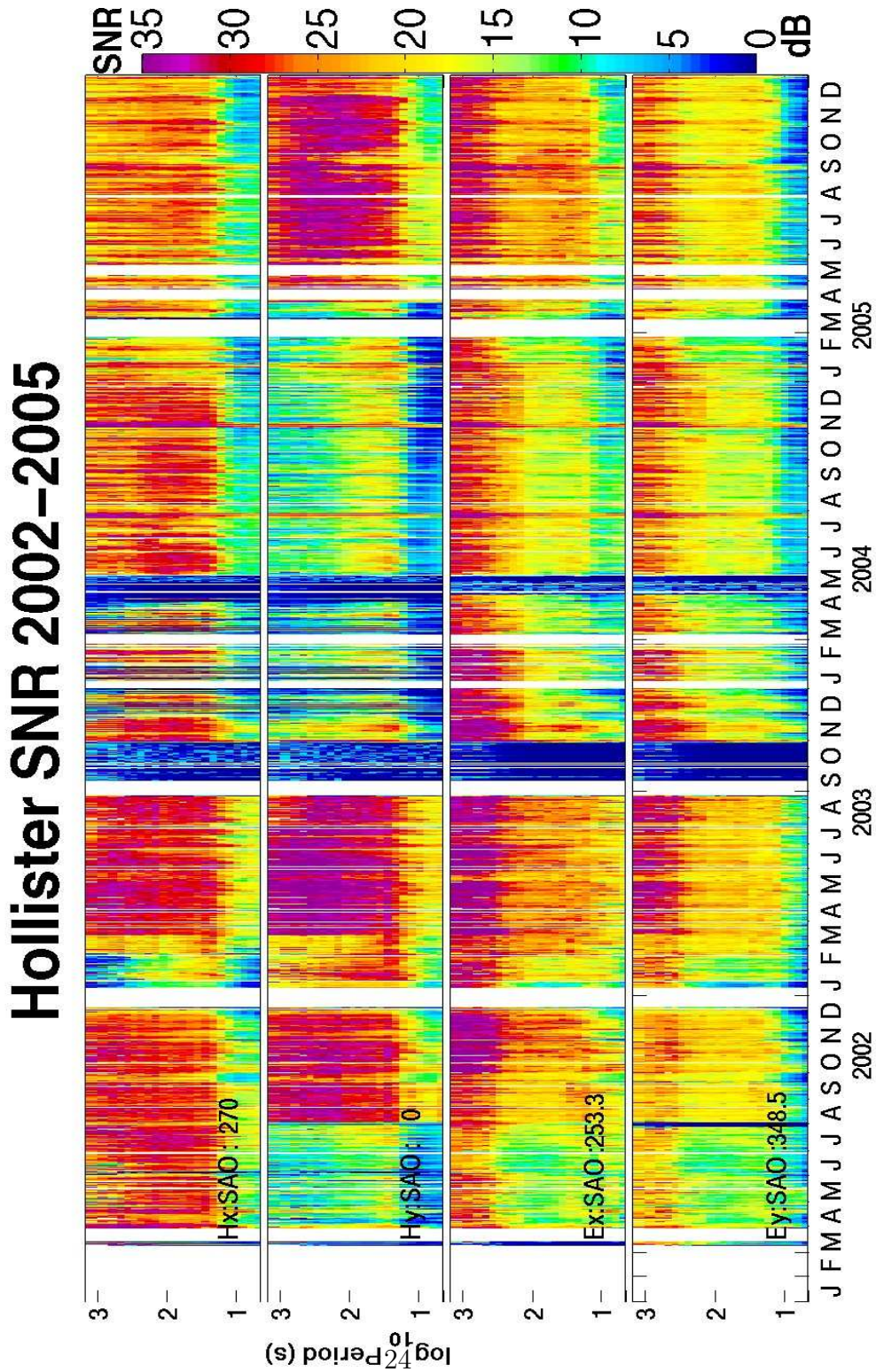

Figure 4: Hollister Electric and Magnetic Field SNRs for four years, including contaminated data

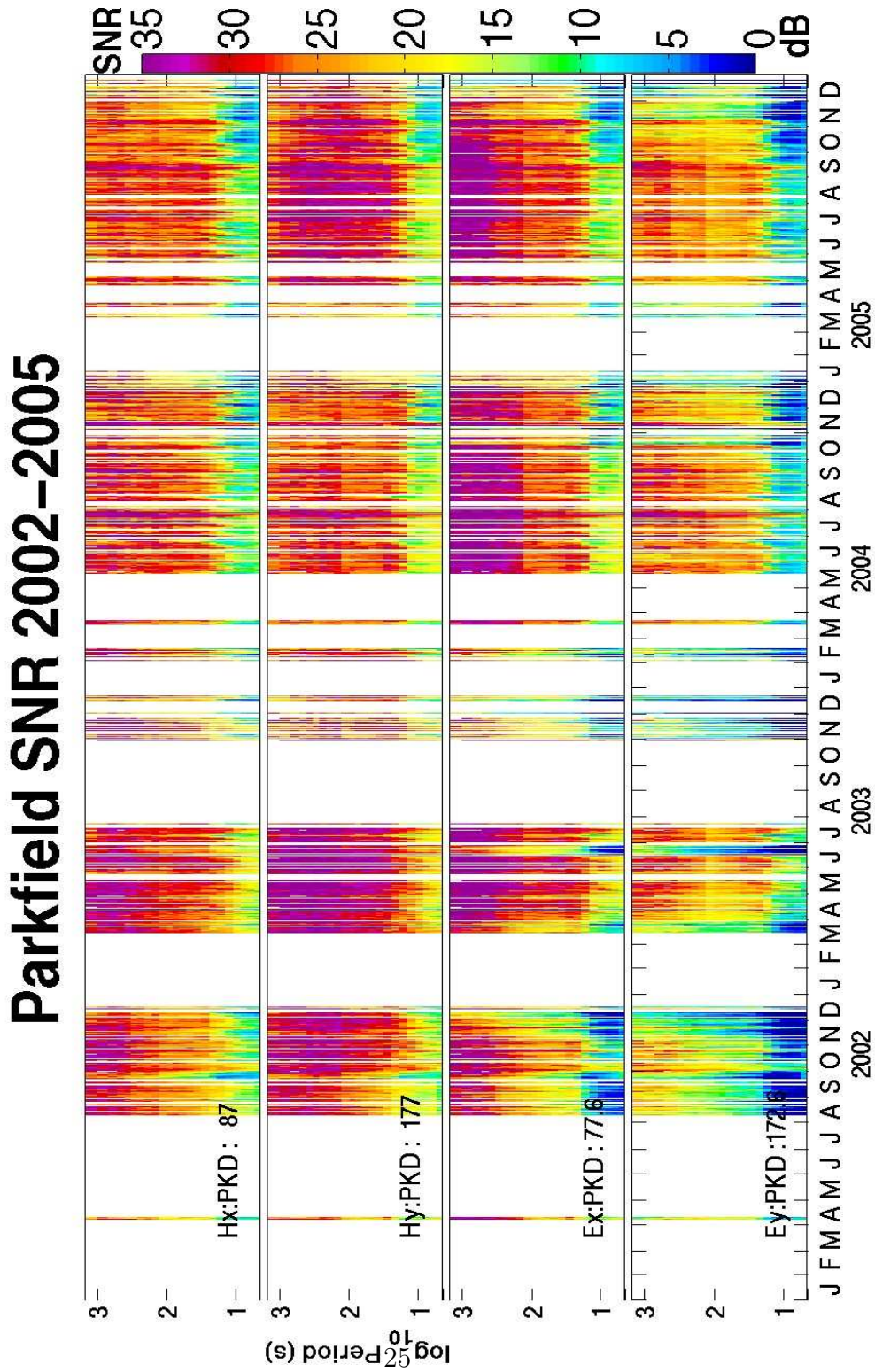

Figure 5: Parfield Electric and Magnetic Field SNRs showing the interesection of good data days on all eight main channels

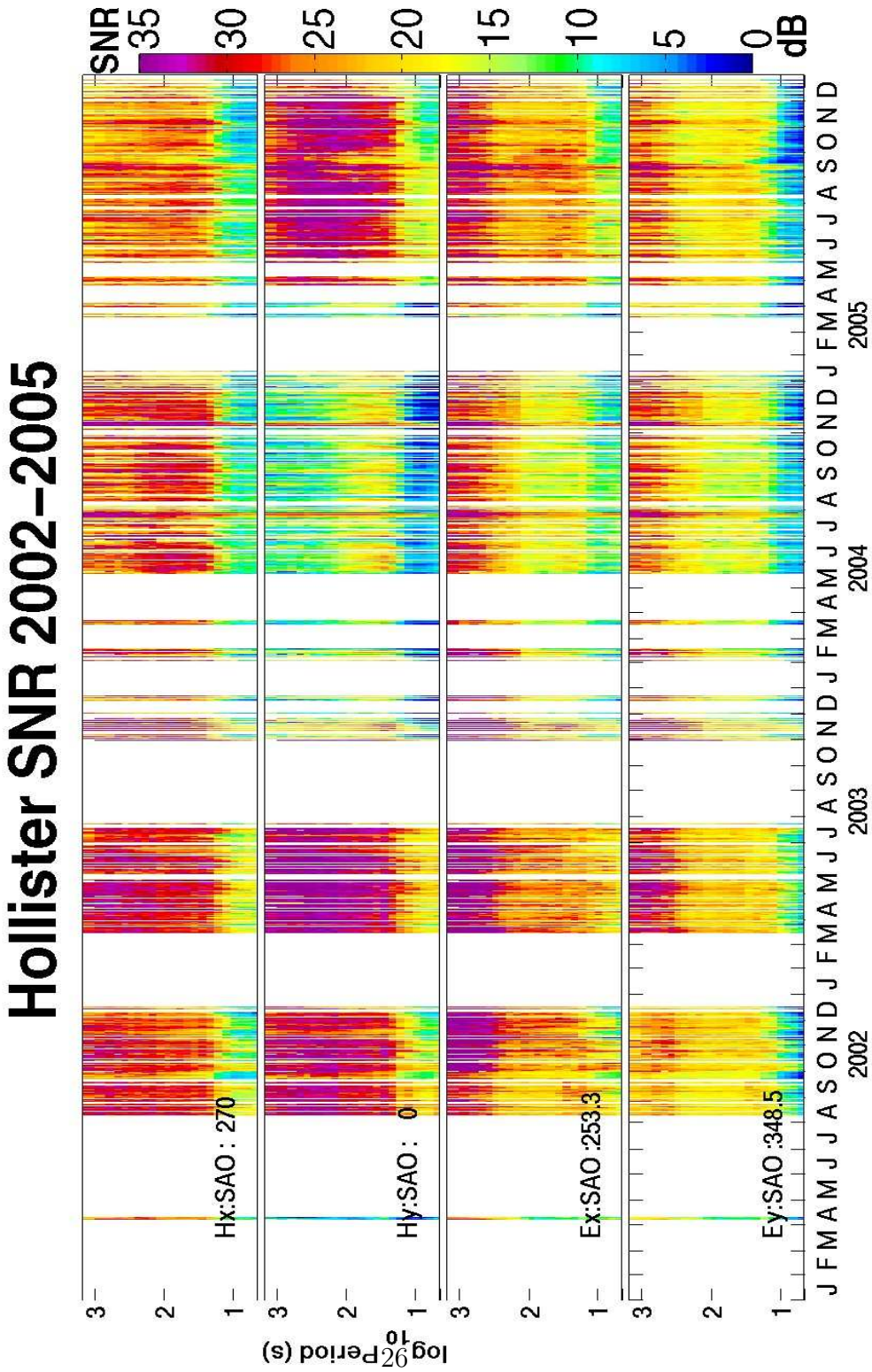

Figure 6: Hollister Electric and Magnetic Field SNRs showing the interesection of good data days on all eight main channels

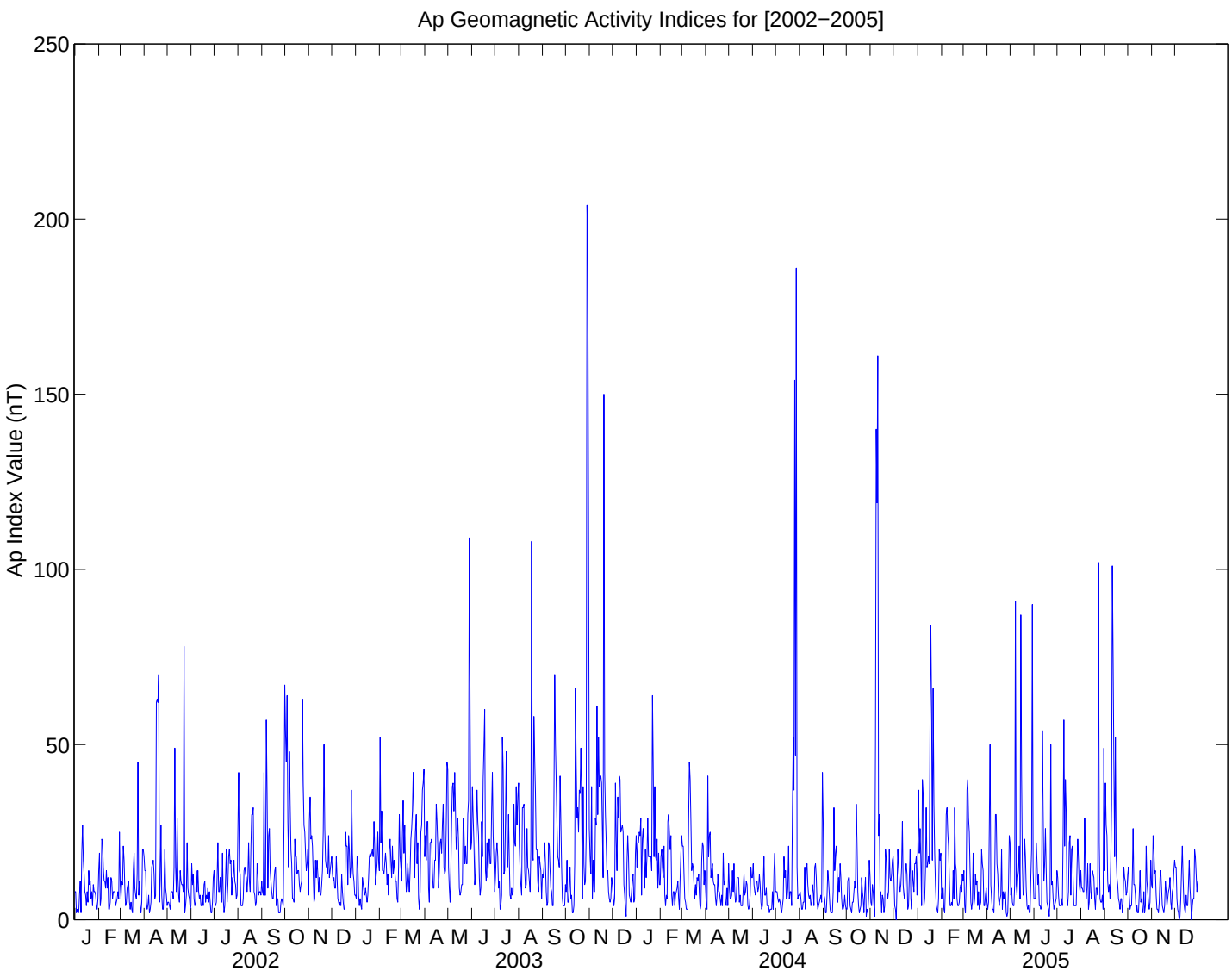

Figure 7: Ap indices showing spikes at SNR global maxima

5 iterations, (where all iterations are performed without intermediate averaging), we show a few example plots from a broadband in the log-middle of our frequency range in Figures 8 and 9, with a phase plots for phase shown in Figures and 10 and 11.

Expressing the apparent resistivity plots in terms of percent deviation from the median it is important that all statistics are performed in linear space wher e they are derived. The data are shifted to linear space and deviation in percent from the median of each band is computed independently. The resulting matr ix is then cleaned up in the same fashion as the other plots. We show a few example plots from a broadband in the higher end of our frequency range in Figure s 12 and 13.

0.5.3 SDM and CCPS and Residuals results

The machinery for the SDM and CC analyses has been developed, but we have yet to interpret the data. Following, we present a few plots derived from the SDM a nd CC data around the mid and high broad frequency bands. As our partitioning of data channels, we treat sets Parkfield and Hollister (CCPS, S for San Andres Geophysical Observatory), as well as electric and magnetic (CCHE). Figures 14, 15, 16, 17 depict eigenvalues one through four res pectively.

Figures 18, 19, 20, 21 depict intersite canonical coherences one through four respectively.

Figures 22, 23, depict intersite canonical coherences one thorugh four respectively.

Finally we include a four year plot of residuals in Figure 24.

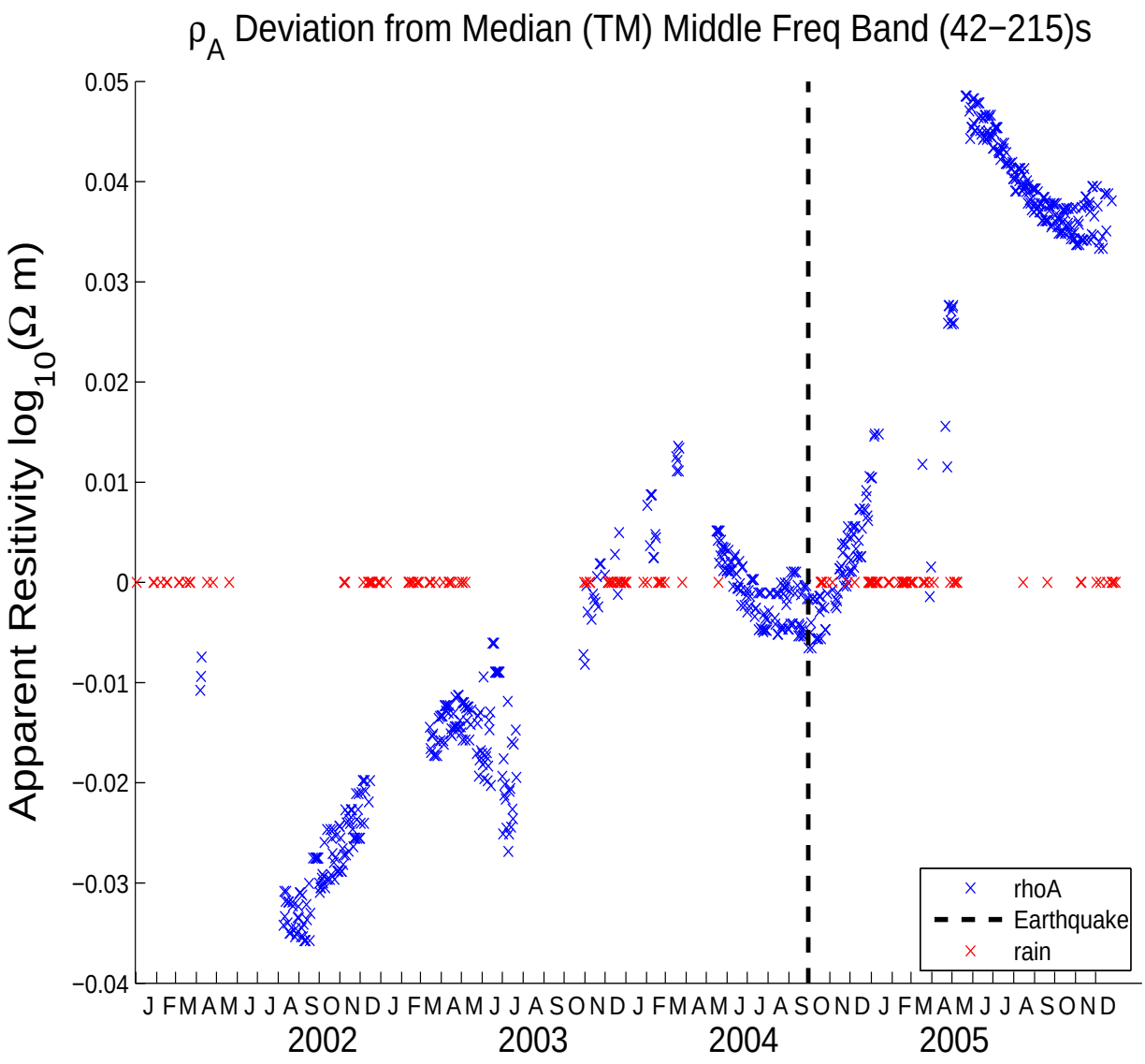

Figure 8: TM mode MF

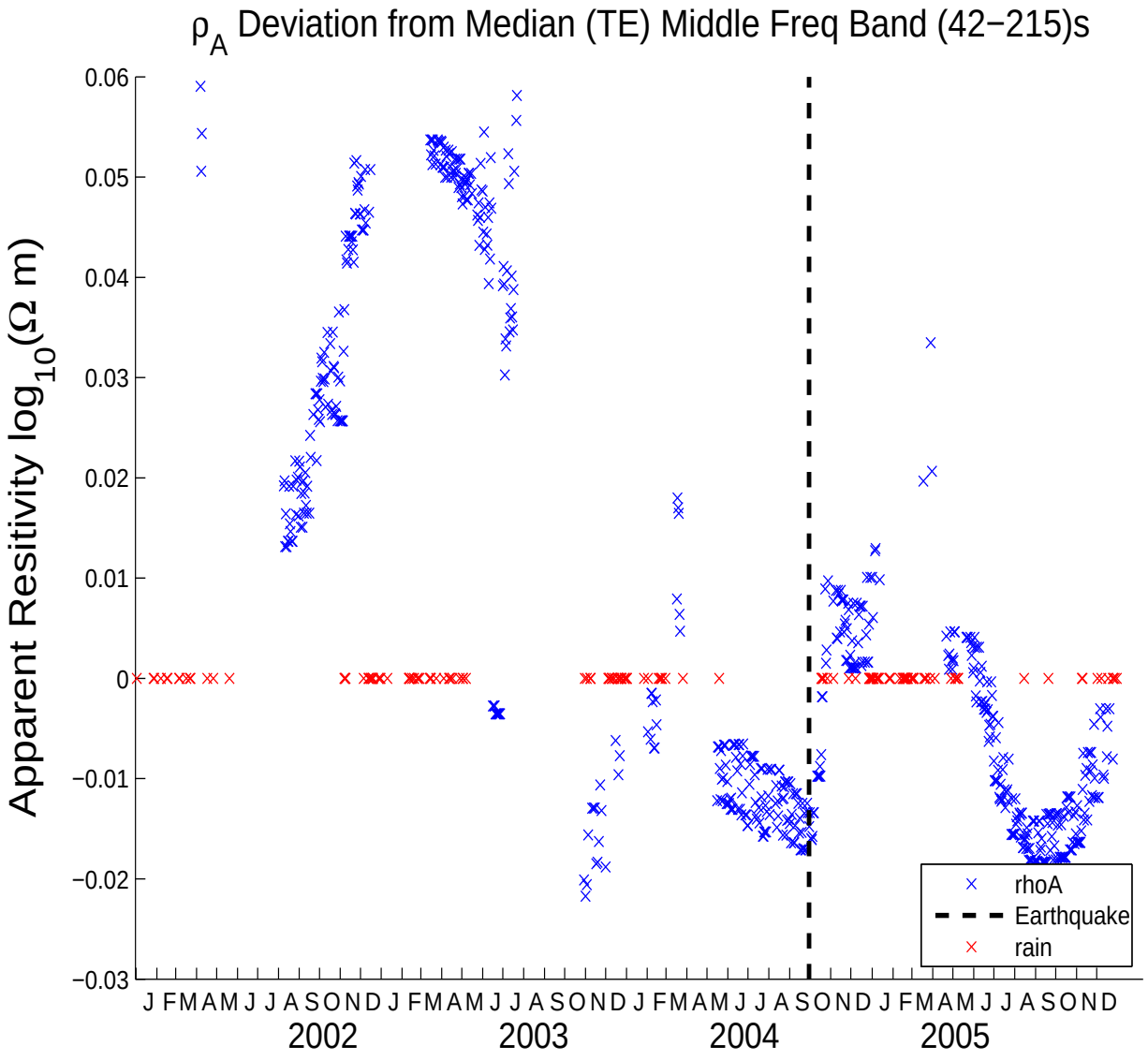

Figure 9: TE mode MF

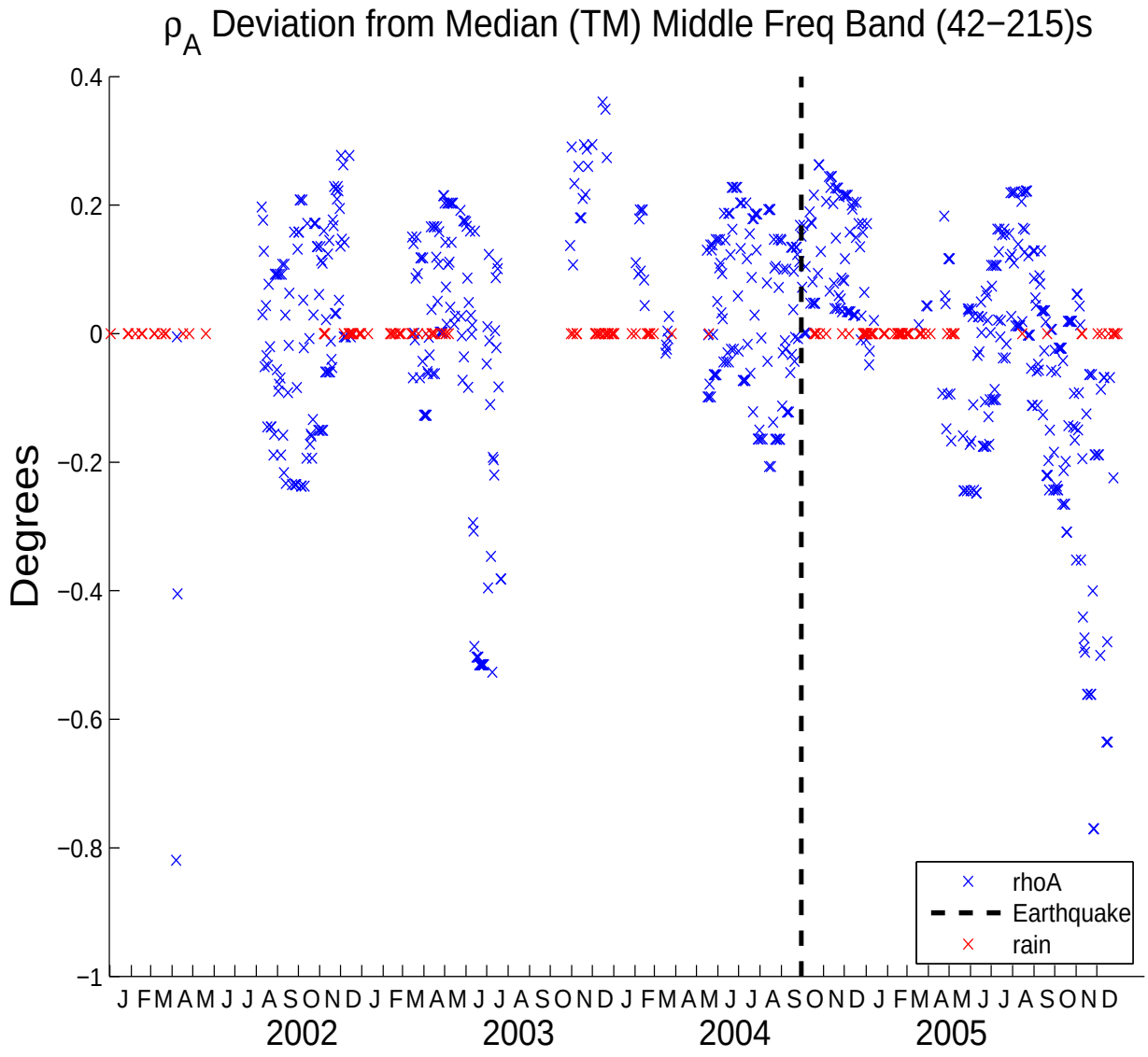

Figure 10: TM mode MF

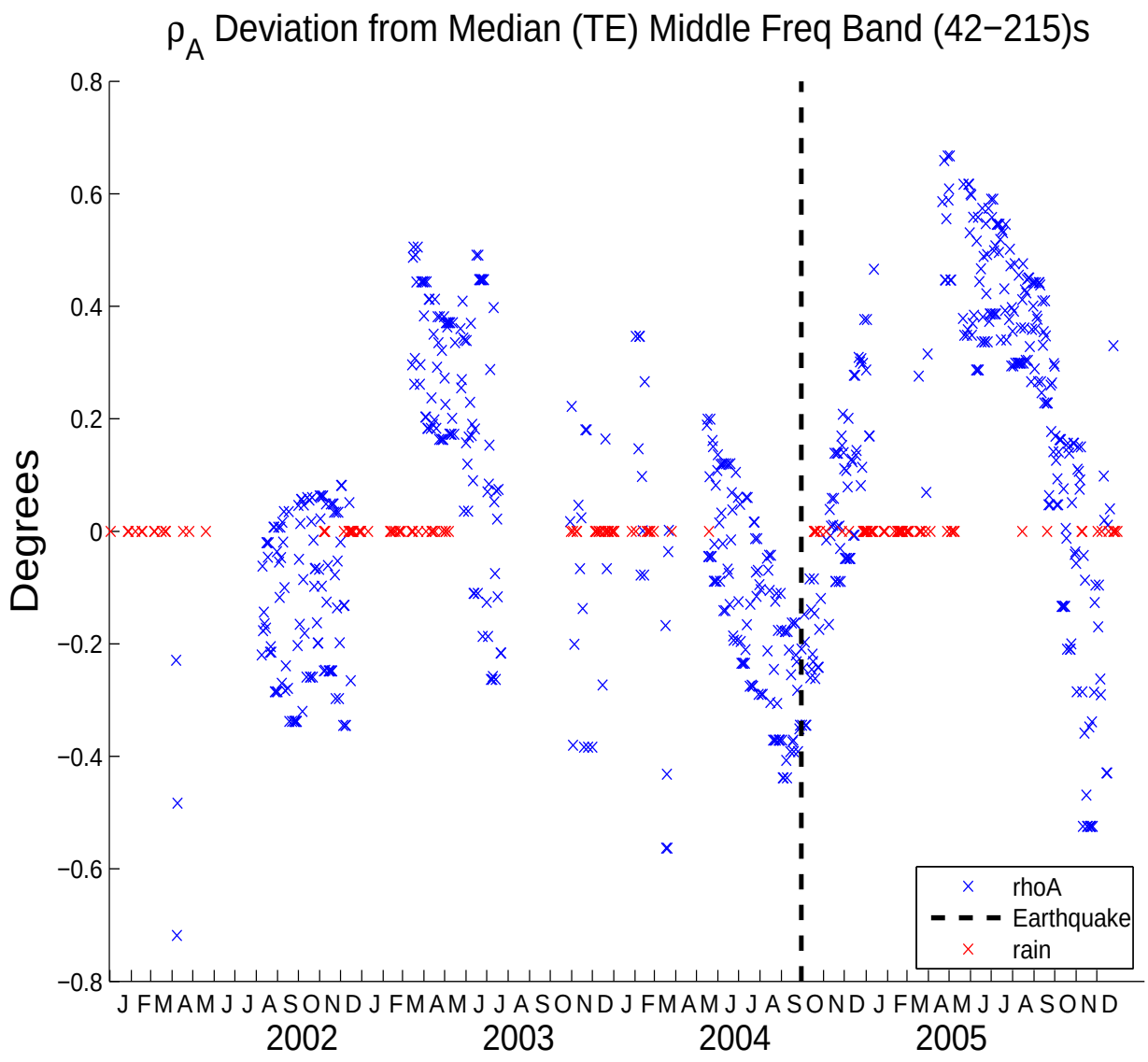

Figure 11: TE mode MF

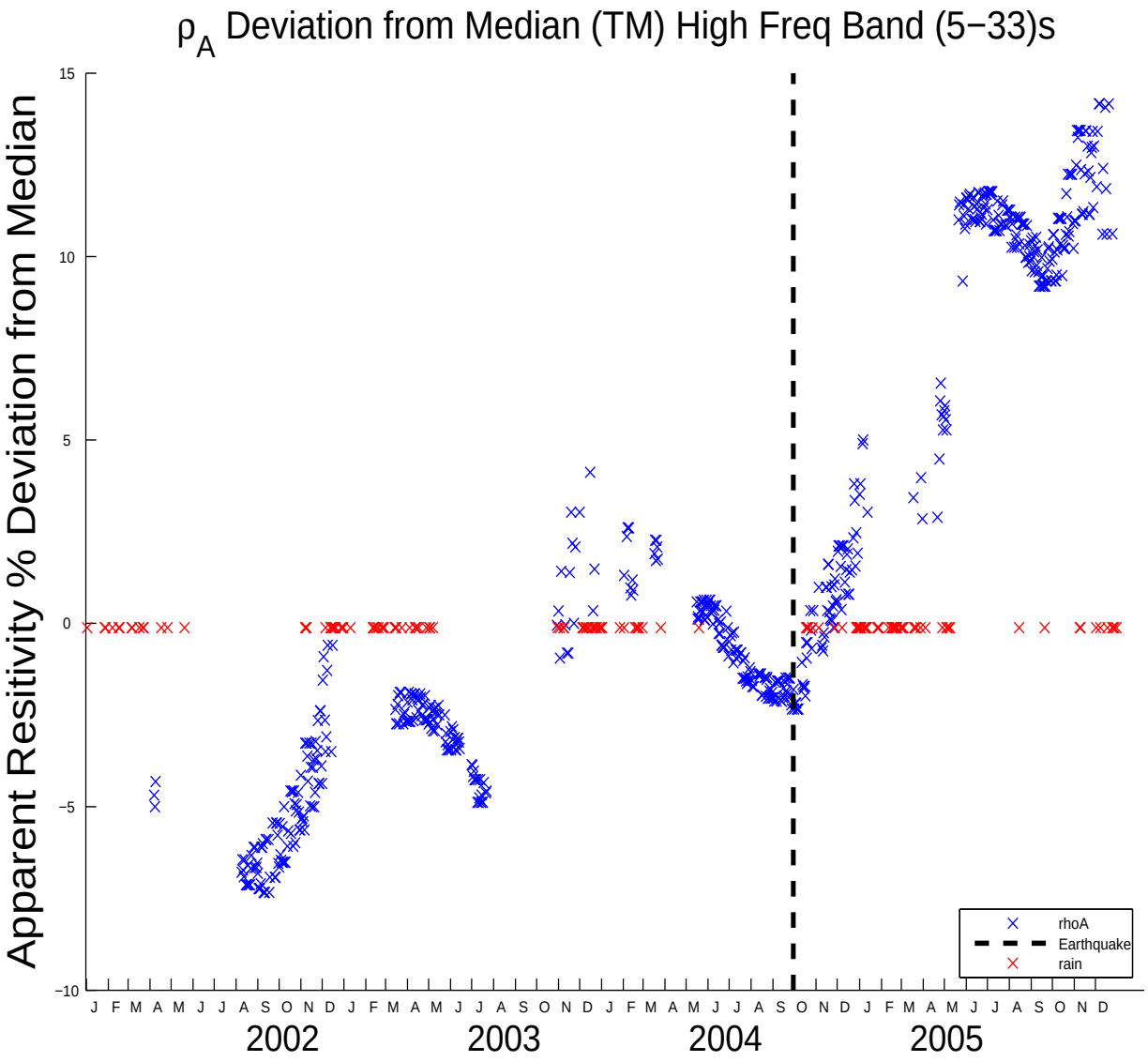

Figure 12: TM mode HF

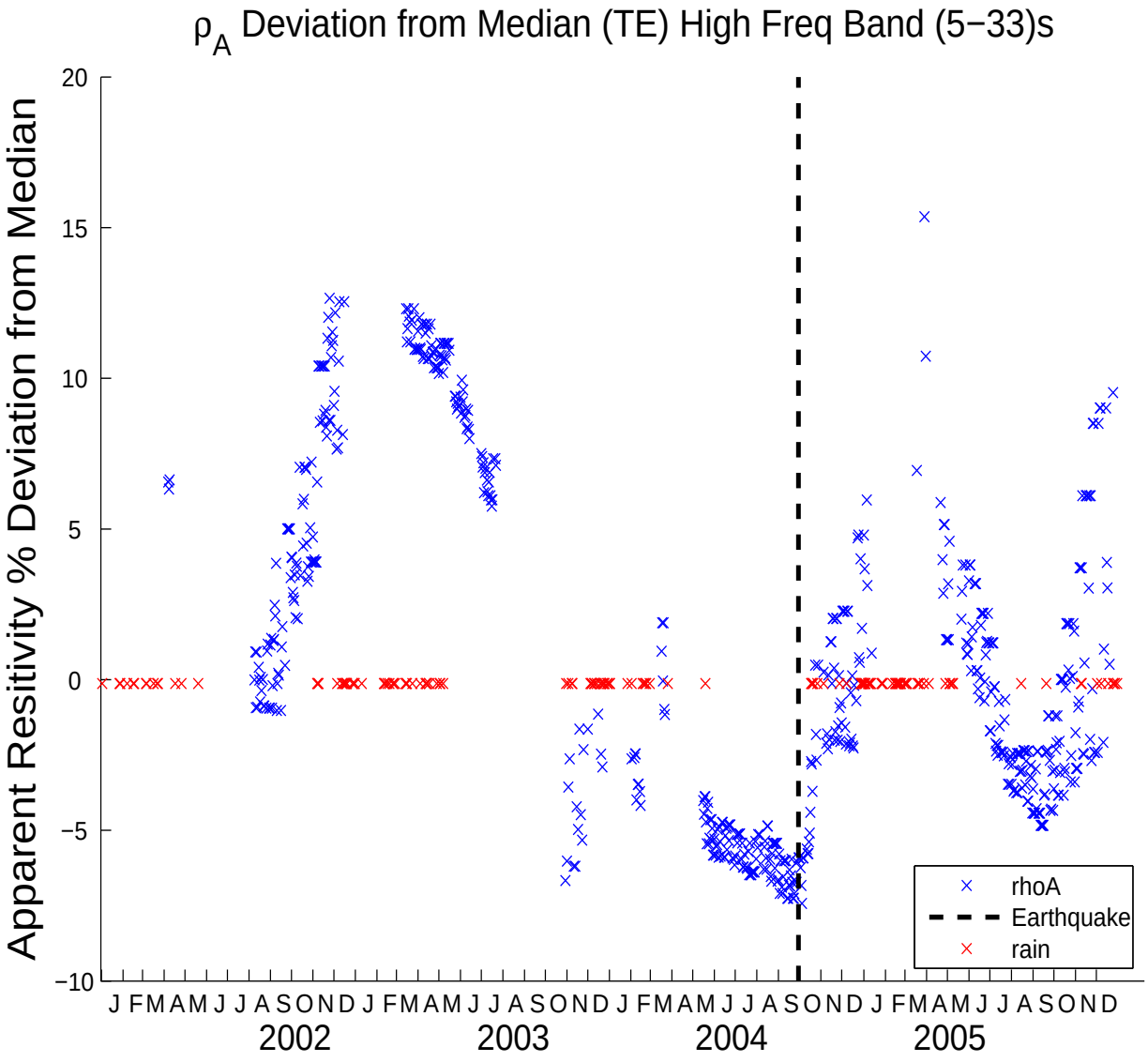

Figure 13: TM mode HF

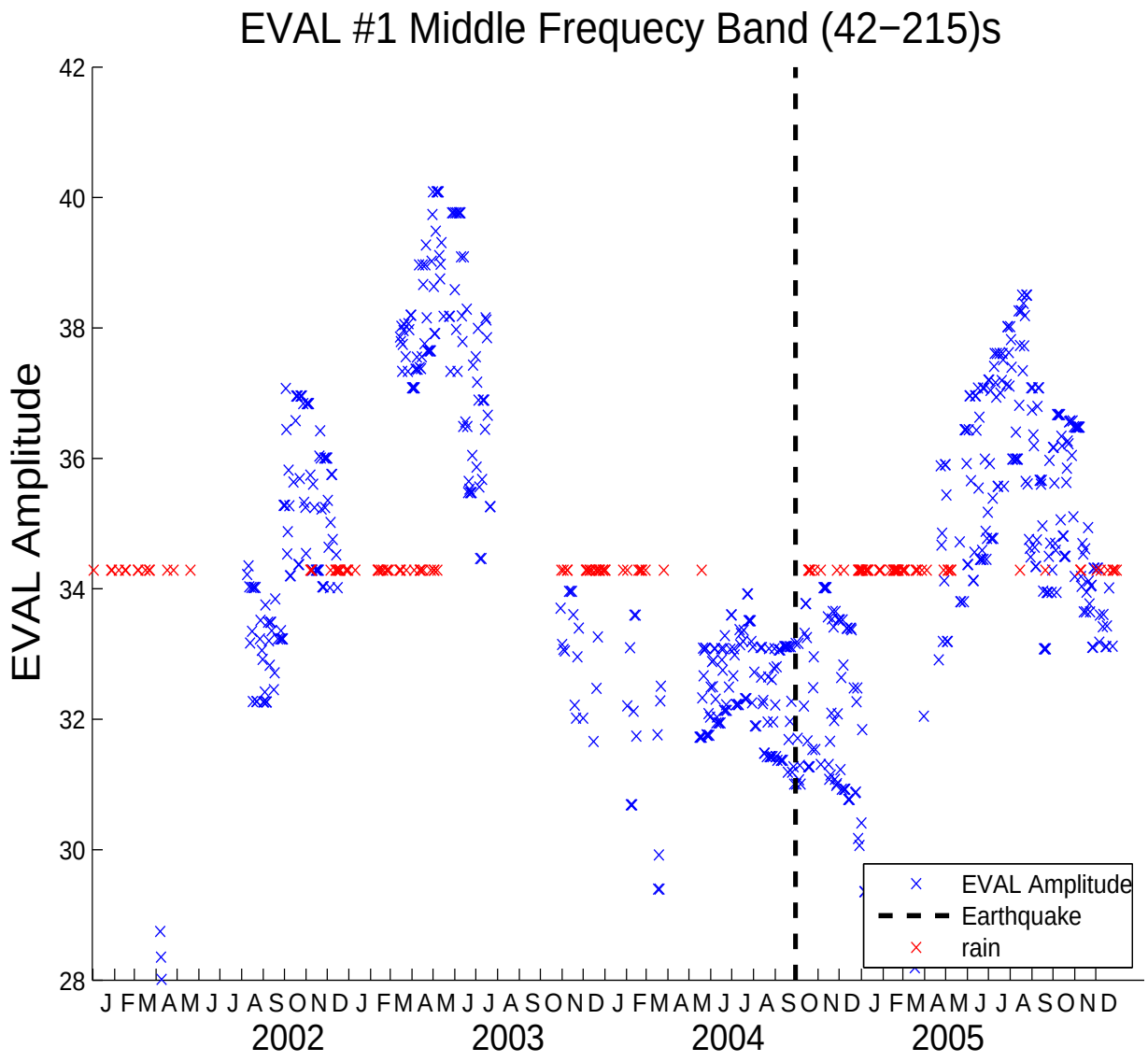
EVAL #1 Middle Frequecy Band (42−215)s
EVAL Amplitude
42
40
38
36
34
32
30
28
J F M A M J J A S O N D J F M A M J J A S O N D J F M A M J J A S O N D J F M A M J J A S O N D
2002
2003
2004
2005
EVAL Amplitude
Earthquake
rain

Figure 14:

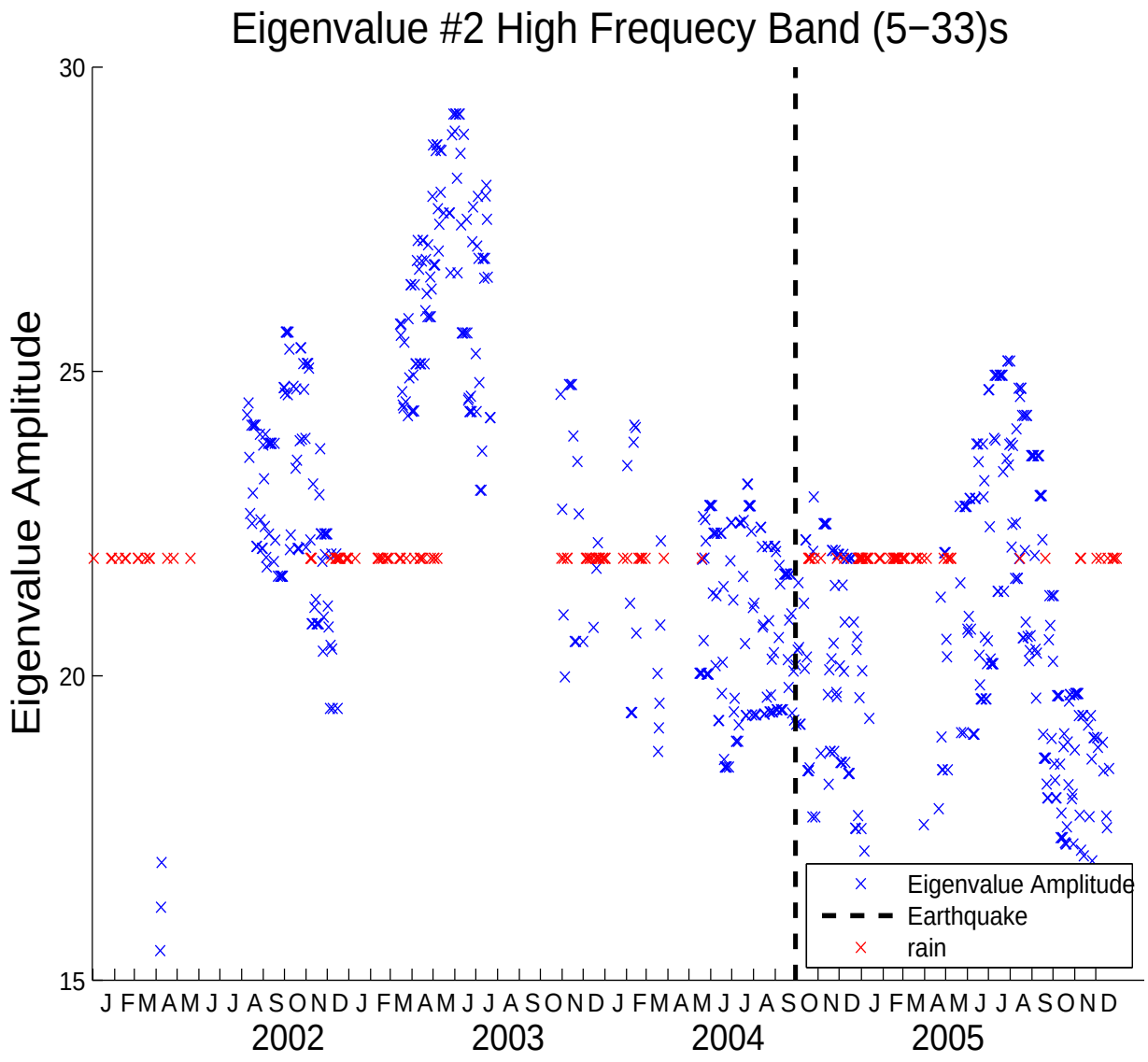
Eigenvalue #2 High Frequecy Band (5−33)s
Eigenvalue Amplitude
30
25
20
15
J F M A M J J A S O N D J F M A M J J A S O N D J F M A M J J A S O N D J F M A M J J A S O N D
2002
2003
2004
2005
Eigenvalue Amplitude
Earthquake
rain

Figure 15:

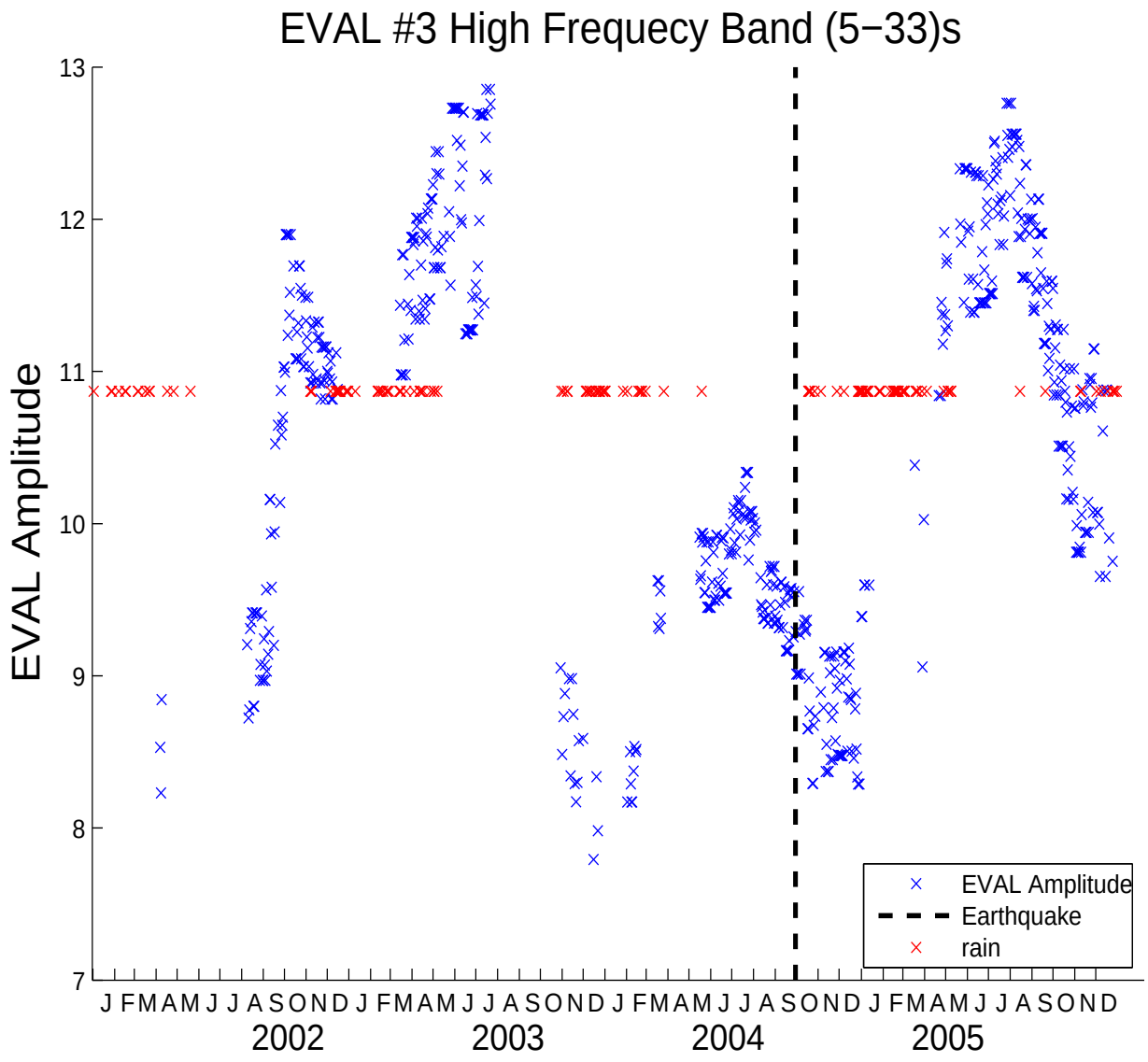
EVAL #3 High Frequecy Band (5−33)s
EVAL Amplitude
13
12
11
10
9
8
7
J F M A M J J A S O N D J F M A M J J A S O N D J F M A M J J A S O N D J F M A M J J A S O N D
2002
2003
2004
2005
EVAL Amplitude
Earthquake
rain

Figure 16:

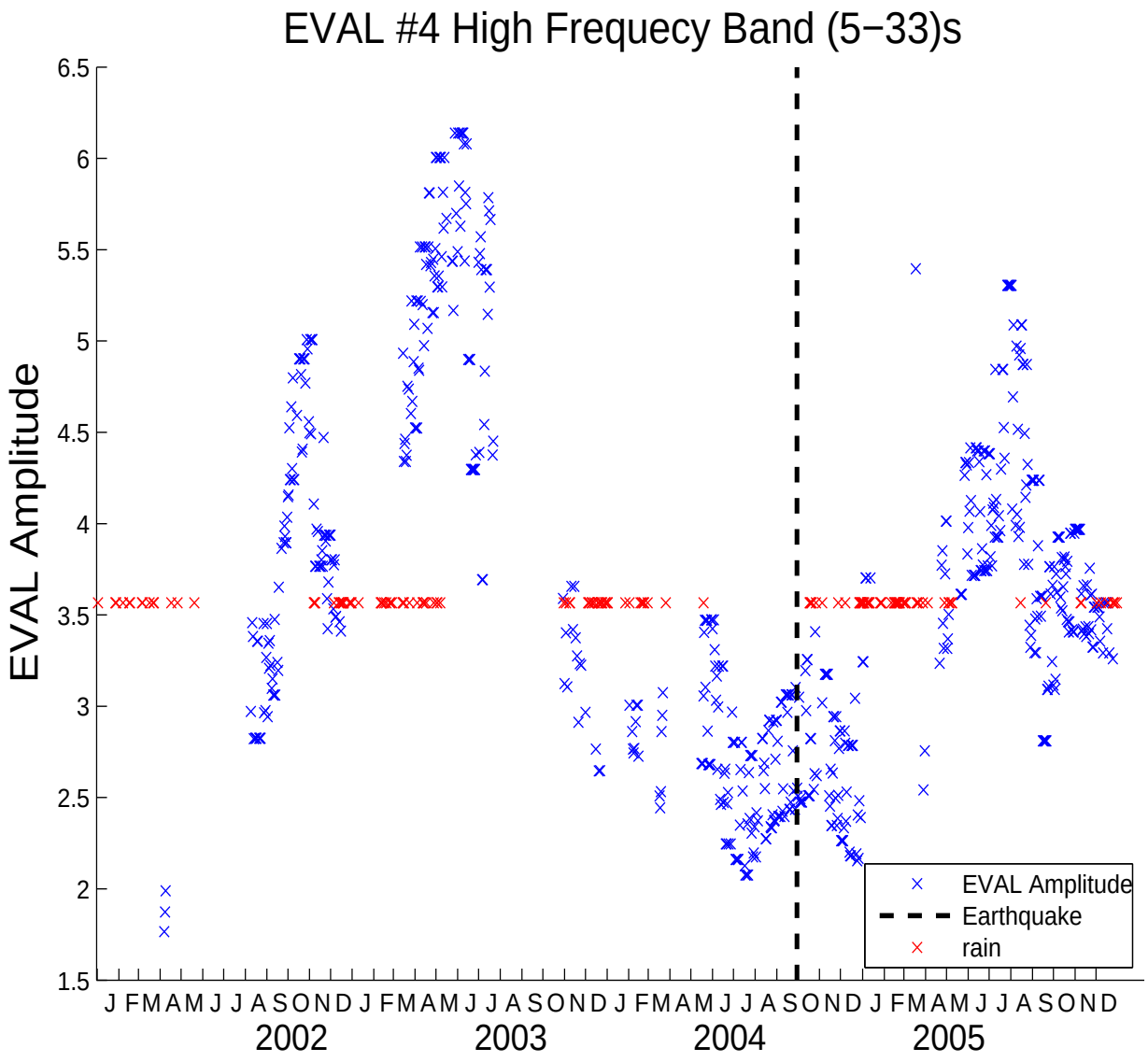
EVAL #4 High Frequecy Band (5−33)s
EVAL Amplitude
6.5
6
5.5
5
4.5
4
3.5
3
2.5
2
1.5
J F M A M J J A S O N D J F M A M J J A S O N D J F M A M J J A S O N D J F M A M J J A S O N D
2002
2003
2004
2005
EVAL Amplitude
Earthquake
rain

Figure 17:

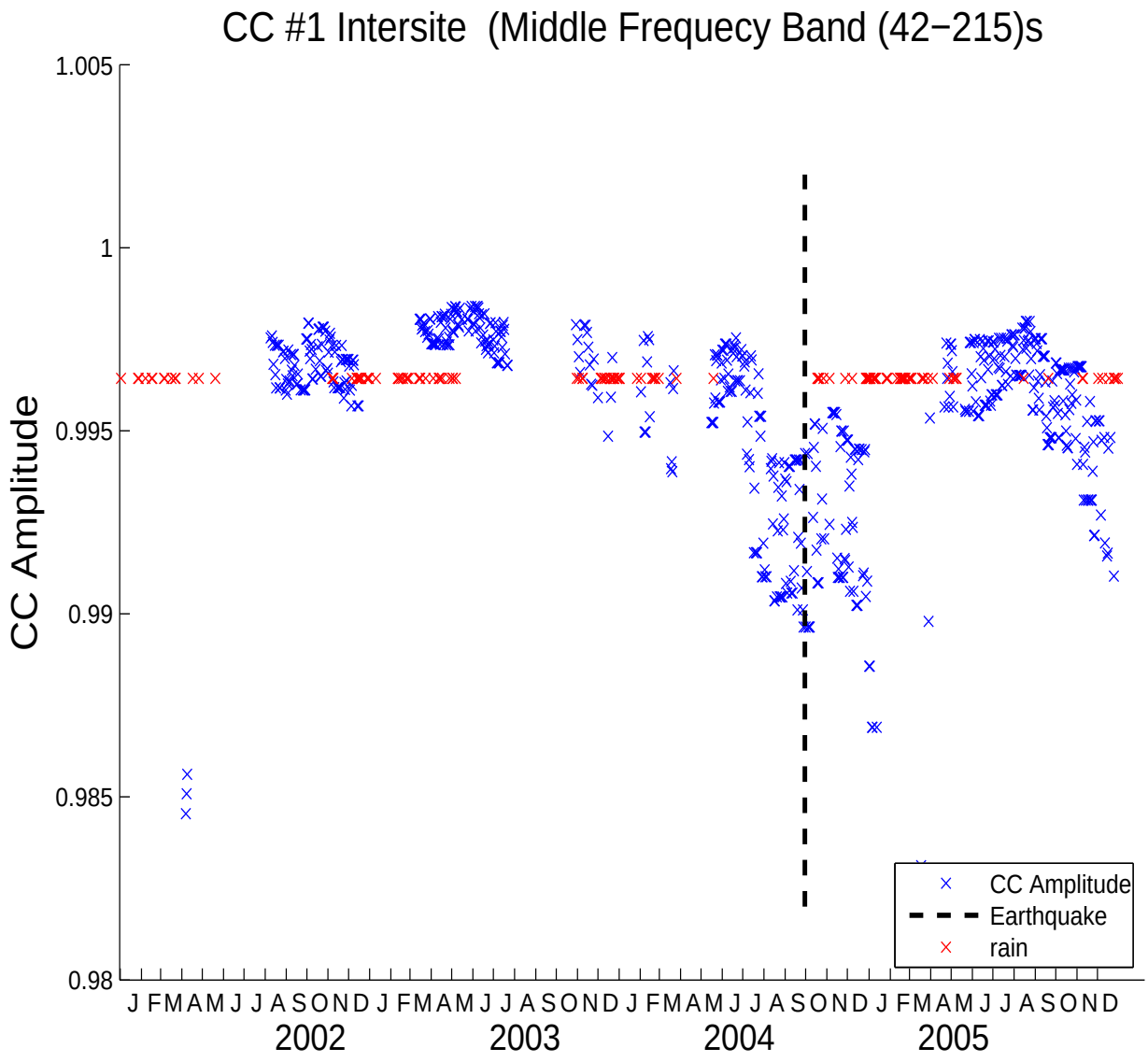
CC #1 Intersite (Middle Frequecy Band (42−215)s
CC Amplitude
1.005
1
0.995
0.99
0.985
0.98
J F M A M J J A S O N D J F M A M J J A S O N D J F M A M J J A S O N D J F M A M J J A S O N D
2002
2003
2004
2005
CC Amplitude
Earthquake
rain

Figure 18:

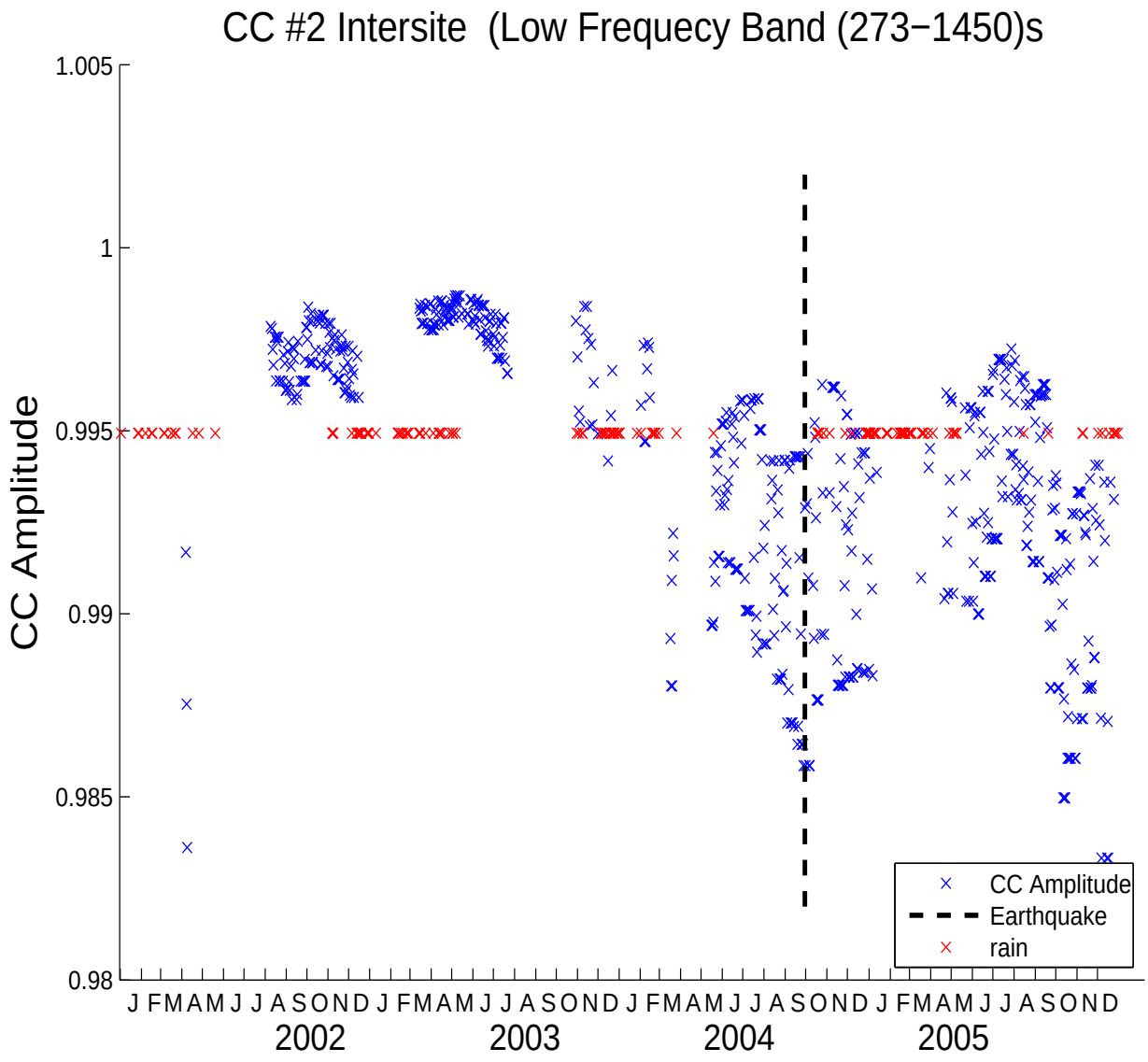
CC #2 Intersite (Low Frequecy Band (273−1450)s
CC Amplitude
1.005
1
0.995
0.99
0.985
0.98
J F M A M J J A S O N D J F M A M J J A S O N D J F M A M J J A S O N D J F M A M J J A S O N D
2002
2003
2004
2005
CC Amplitude
Earthquake
rain

Figure 19:

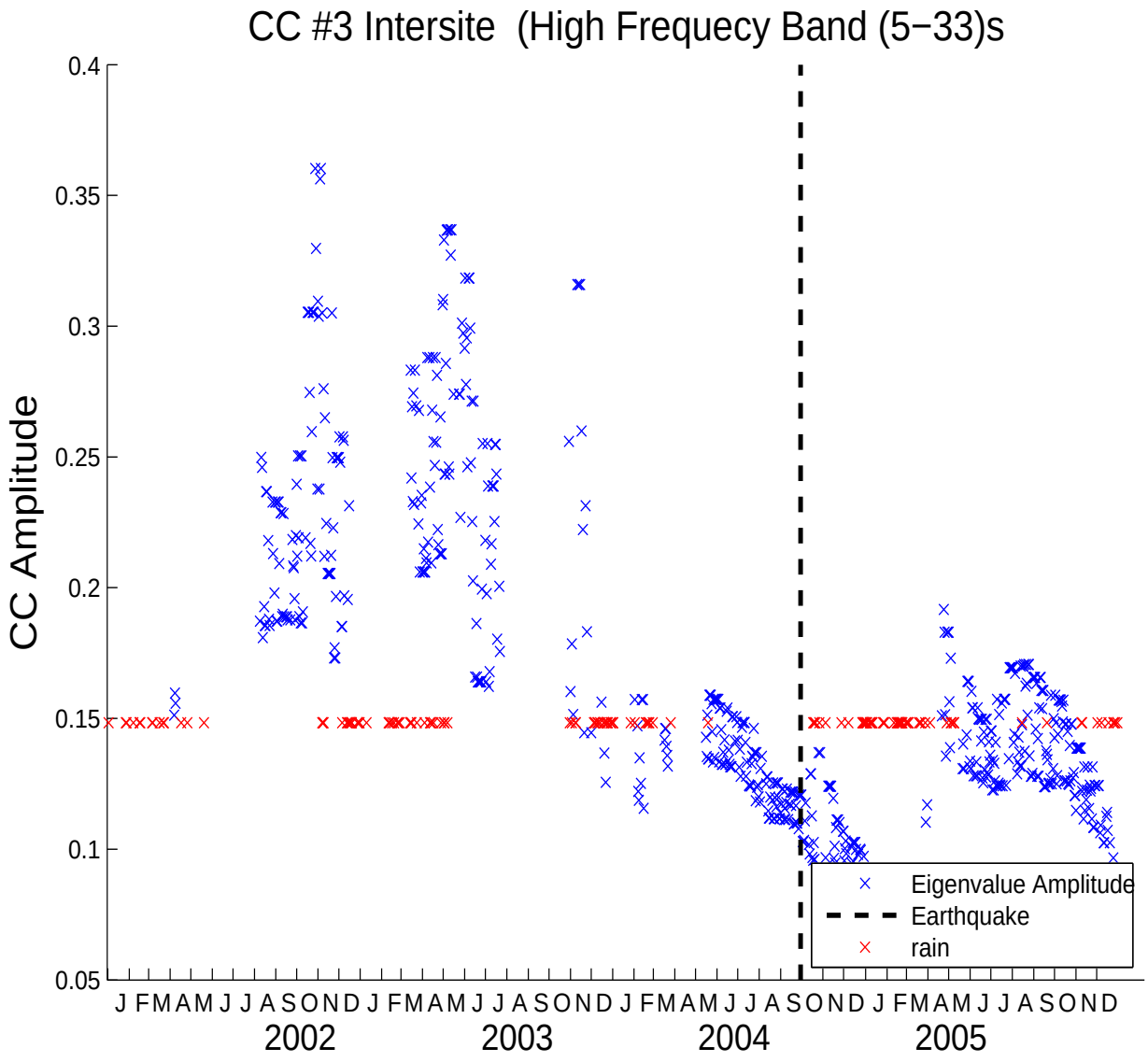
CC #3 Intersite (High Frequecy Band (5−33)s
CC Amplitude
0.4
0.35
0.3
0.25
0.2
0.15
0.1
0.05
J F M A M J J A S O N D J F M A M J J A S O N D J F M A M J J A S O N D J F M A M J J A S O N D
2002
2003
2004
2005
Eigenvalue Amplitude
Earthquake
rain

Figure 20:

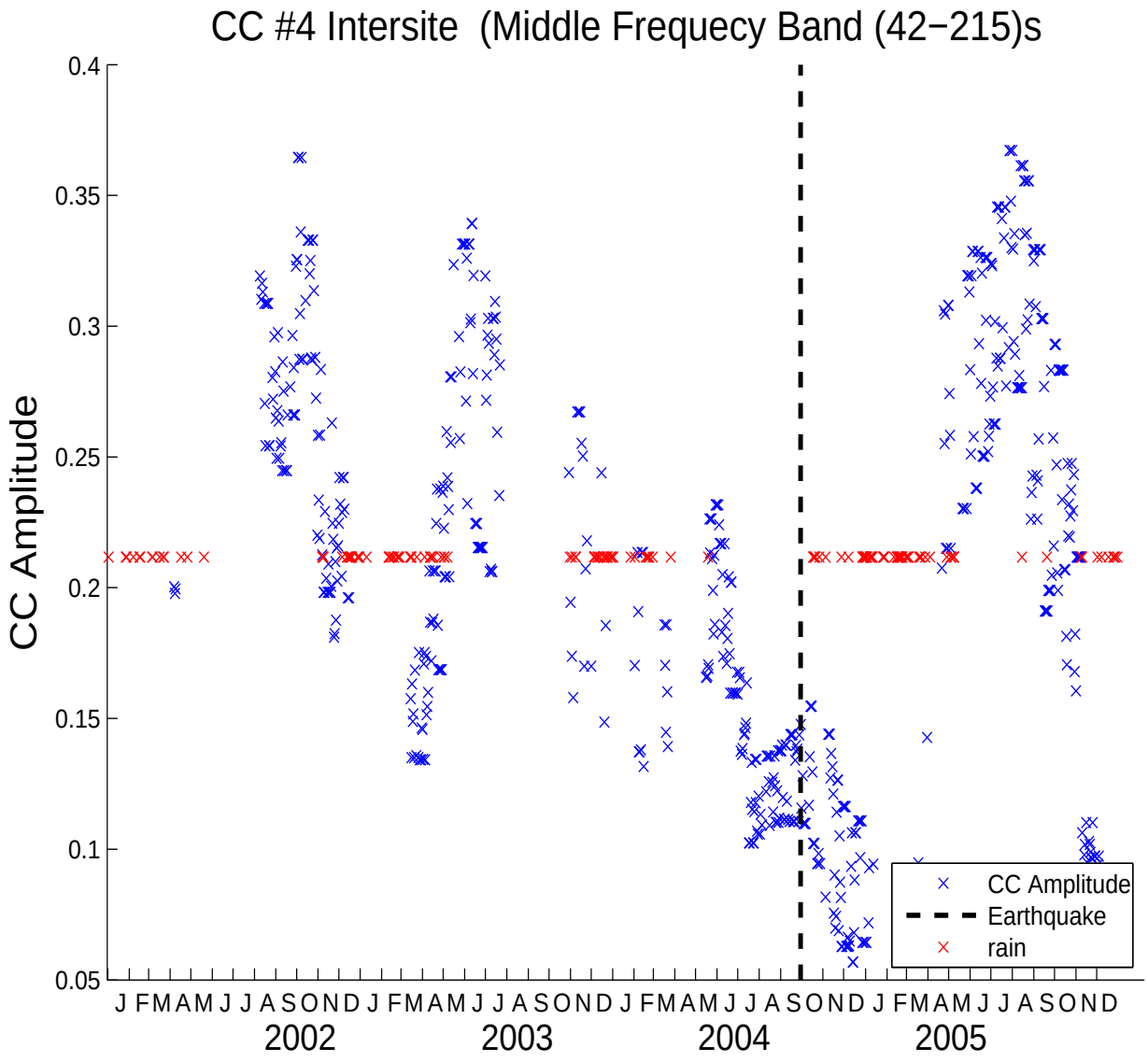
CC #4 Intersite (Middle Frequecy Band (42−215)s
CC Amplitude
0.4
0.35
0.3
0.25
0.2
0.15
0.1
0.05
J F M A M J J A S O N D J F M A M J J A S O N D J F M A M J J A S O N D J F M A M J J A S O N D
2002
2003
2004
2005
CC Amplitude
Earthquake
rain

Figure 21:

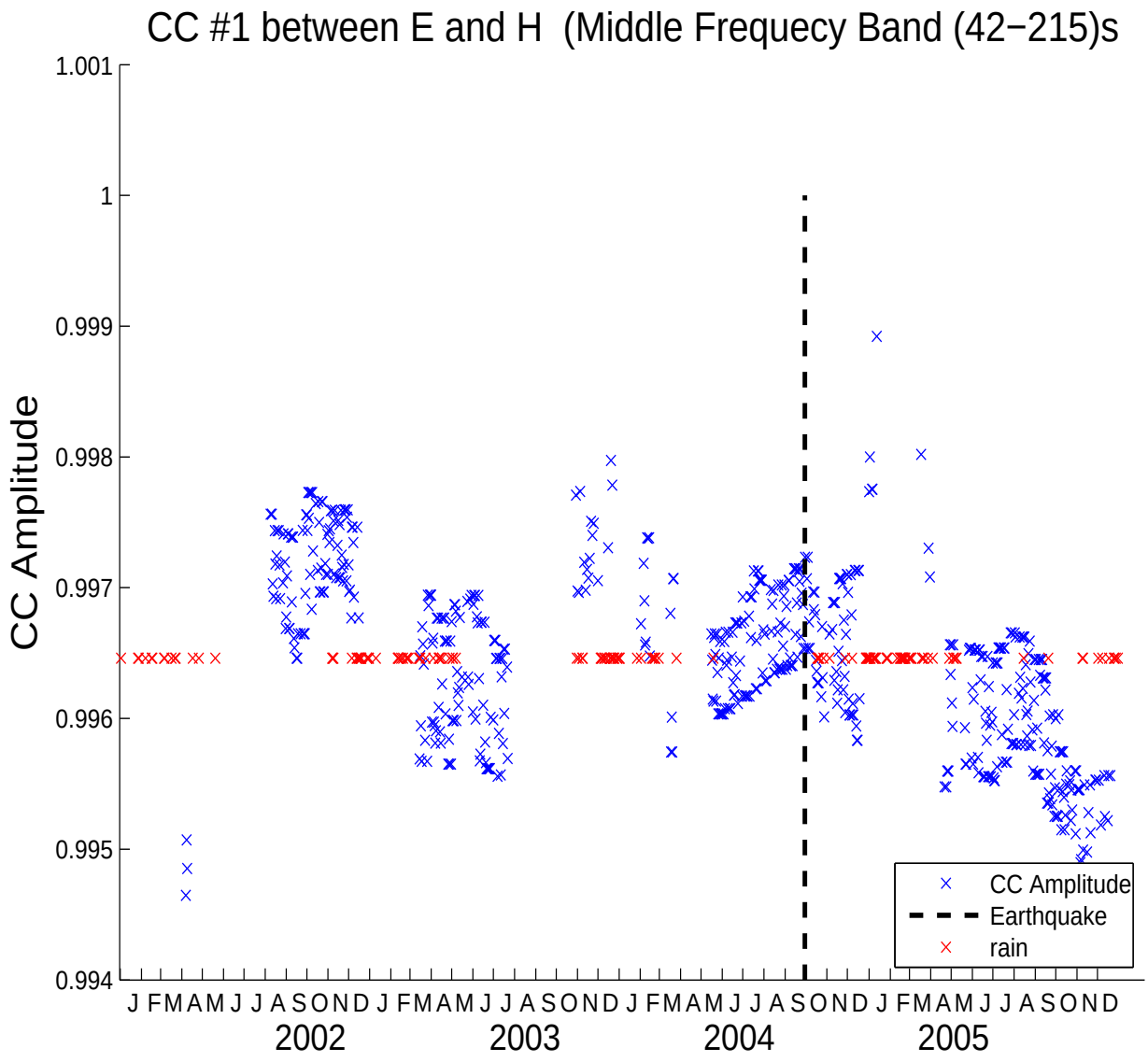
CC #1 between E and H (Middle Frequecy Band (42−215)s
CC Amplitude
1.001
1
0.999
0.998
0.997
0.996
0.995
0.994
J F M A M J J A S O N D J F M A M J J A S O N D J F M A M J J A S O N D J F M A M J J A S O N D
2002
2003
2004
2005
CC Amplitude
Earthquake
rain

Figure 22:

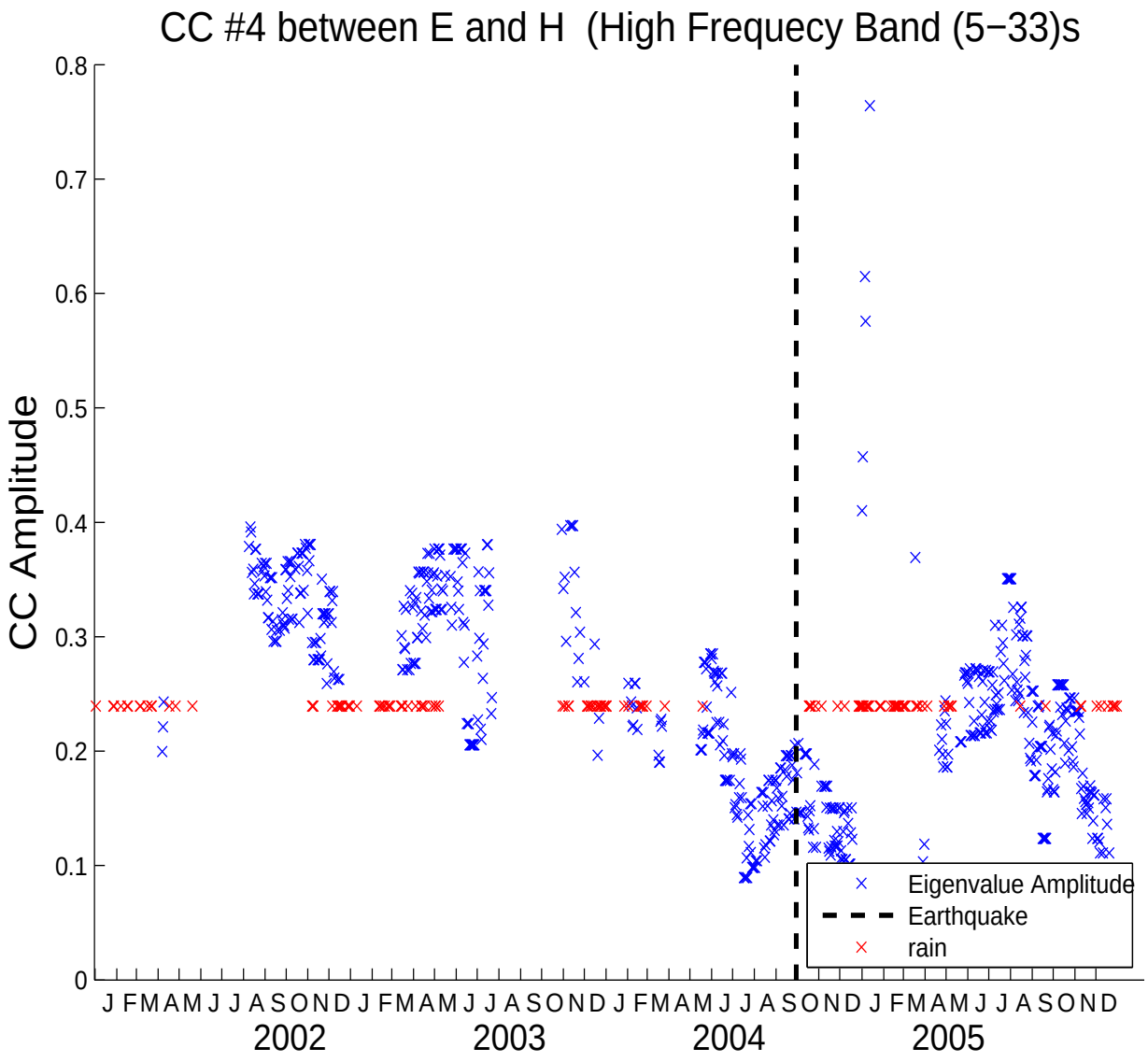
CC #4 between E and H (High Frequecy Band (5−33)s
CC Amplitude
0.8
0.7
0.6
0.5
0.4
0.3
0.2
0.1
0
J F M A M J J A S O N D J F M A M J J A S O N D J F M A M J J A S O N D J F M A M J J A S O N D
2002
2003
2004
2005
Eigenvalue Amplitude
Earthquake
rain

Figure 23:

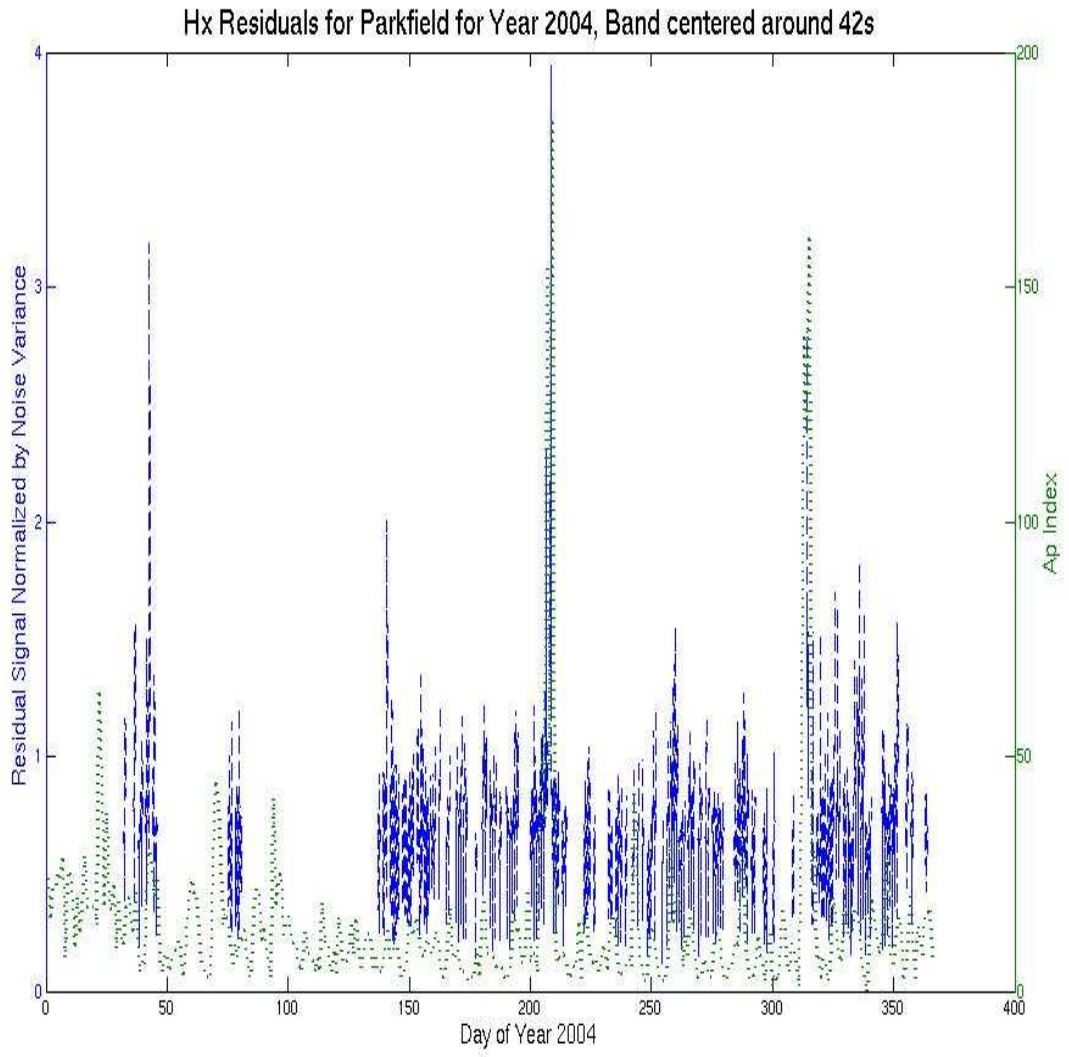

Figure 24: Residual data for 2004 Hx PKD

0.6 Future Work

The above report constitutes a summary of some of our results from examining the Parkfield-Hollister EM data. This report is on a project in progress and we plan to augment our report with the following before submitting a peer-reviewed publication. The concluding processing will include MA indices from NCEDC data. These provide a direct comparison to the published figures of *Fraser-Smith et. al.* (1990) with respect to fields observed around the time of an earthquake. A magnetotelluric distortion analysis is planned to interpret the long term variations in apparent resistivity, possibly in terms of seasonal variation in near-surface distortion effects. The use of CC processing as a remote reference method compared with the standard method of calculating residuals is planned. Once the residuals are obtained a statistical analysis of outliers will be performed.

In addition to calculating residuals in the way described above (standard Remote Reference Processing) we have developed software to calculate residuals via a different scheme involving Canonical Coherences. The basic method involves obtaining a set of vectors C representing the median canonical coherence vectors between sites on to the Principal Component representations of the data at a single site. The residual TS obtained using this method should represent all data observed which are not coherent between sites. This is a different method and promises to be more robust at removing natural fields in a case where multiple sites are being considered.

0.7 References

Berdechevsky M.N., Dmitriev V.I., (2002), Magnetotellurics in the Context of Ill-Posed Problems, Sociey of Exploration Geophysicists

Bernardi, A., Fraser-Smith, A.C., Villard Jr., O.G., 1989, Measurements of BART Magnetic Fields with an Automatic Geomagnetic Pulsation Index Generator, IEEE Transactions on Electromagnetic Compatibility, vol.31, no. 4, p413-417

Brillinger, D. R., 1975, Time Series, Data Analysis and Theory, Holt Rinehart and Winston Inc, ISBN 0-03-076975-2

Corwin R.F., Morrison H.F. (1977), Self-Potential Variations Preceding Earthquakes in Central California, Geophysical Research Letters Vol. 4, No. 4 pp171-174 Egbert, G.D., Booker, J.R., (1986), Robust estimation of geomagnetic transfer functions, Geophys. J. R. astr. Soc., v.87, pp173-194

Egbert, G.D., Booker, J.R., (1989), Multivariate Analysis of Geomagnetic Array Data 1. The Response Space, Journal of Geophys. Res. V94 No.B10 pp14227-14247

Egbert, G.D., (1989), Multivariate Analysis of Geomagnetic Array Data 2. Random Source Models, Journal of Geophys. Res. V94 No.B10 pp14249-14265

Egbert G. D. (1997), Robust multiple-station magnetotelluric data processing, Geophys. J. Int. 130, pp475-496

Egbert G. D. (2005), Final TEchnical Report to USGS–03HQGR0060

Eisel M., Egbert G.D., (2001), On the stability of magnetotelluric transfer function estimates and the reliability of their variances, Geophys. J. Int., 144, pp65-82

Fenoglio, M.A., Fraser-Smith, A.C., Beroza, G.C., Johnston, M.J.S., (1993), Comparison of Ultra-Low Frequency Electromagnetic Signals with Aftershock Activity During the 1989 Loma Prieta Earthquake Sequence, Bull. Seis. Soc. America, Vol. 83, No2, pp347-357

Fitterman, D. and Madden, T. (1977). Resistivity observations during creep events at Melendy Ranch, California. Journal of Geophysical Research 82(B33)

Fraser-Smith, A. C., Bernardi, A., McGill, P. R., Ladd, M. E., Helliwell, R. A., and Villard, O. G., 1990, Low-frequency magnetic field measurements near the epicenter of the Ms 7.1 Loma Prieta Earthquake, Geophys. Res. Lett., 17, 1465-1468.

Fraser-Smith A.C., McGill P.R., Helliwell R.A., Villard Jr. O.G., Ultra-low frequency magnetic field measurements in southern California during the Northridge earthquake of 17 January 1994, Geophysical Research Letters, Vol. 21, No. 20, pp2195-2198

Gamble T.D., Goubau W.M., Clarke J. (1979), Magnetotellurics with a remote reference, Geophysics, 44, pp53-68

*Geller R.J., (1996) Debate on Evaluation of the VAN Method: Editors Introduction, Geophysical Reearch Letters, Vol. 23, No. 11 pp1291-1293 this entire issue is devoted to the VAN method controversy

Hayakawa M., Molchanov O., Tronin A., Hobara Y., Kodama T (2001), NASDA's Earthquake Remote Sensing Frontier Research Seismo-Electromagnetic Phenomena in the Lithosphere, Atmosphere, and Ionosphere, Final Report March 2001, The University of Electro-Communications, Chofu, Tokyo, Japan

Hamada, K., Statistical evaluation of the SES predictions issued in Greece:alarm and success rates, Tectonophysics, 224 (1993) 203-210

Hyvarinen, A., Karhunen, J., Oja, E., (2001) independent Componenets Analysis, Wiley Interscience, ISBN 0-471-40540-X

Johnston, M. J., Sasai, Y., Egbert, G.D., Kappler, K. 2005, Seismo-magnetic Effects from the Long-awaited September 28, 2004, M6 Parkfield Earthquake, AGU paper Fall Meeting 2005.

Kagan, Y. Y. 1996 VAN earthquake predictions: An attempt at statistical evaluation Geophys. Res. Lett. Vol. 23 , No. 11 , p. 1315-1318 (95GL03417)

Kappler, K.N., Egbert, G.D., Morrison, H.F., 2005, Long Term Monitoring of EM Signals Near Parkfield CA, AGU paper Fall Meeting 2005

Karakelian D., Beroza G.C., Klemperer S.L., Fraser-Smith A.C. (2002), Analysis of Ultralow-Frequency Electromagnetic Field Measurements Associated with the 1999 M 7.1 Hector Mine, California, Earthquake Sequence, Bulliten of the Seismological Society of America, Vol. 92, No. 4

Kopytenko Y.A., Ismaguilov V.S., Molchanov O.A., Kopytenko E.A., Voronov P.M., Hattori K., Hayakawa M., Zaitzev D.B. (2002), Investigation of ULF magnetic disturbances in Japan during seismic active period, Journal of Atmos. Elec., Vol. 22, No. 3, pp207-215

Lyubushin Jr., A. A. (1998), Analysis of Canonical Coherences in the Problems of Geophysical Monitoroing, Izvestiya, Physics of the Solid Earth, Vol 34, No 1, pp52-58

Ma, Q., Feng, Z., Song, Z., Zhao, W. (2004), Study on the variation characteristics of the geoelectirc field preceding earthquakes, Acta Seismologica Sinica, Vol 17, No.3, pp334-343

Mazella, A.,Morrison, H. F., 1974, Electrical resistivity variations associated with earthquakes on the San Andreas Fault:Science, 185, 855-857.

Molchanov O.A., Y.A. Kopytenko, P.M. Voronov, E.A. Kopytenko, T.G. Matiashvili, A.C. Fraser-Smith, A. Bernardi (1992), Results of ULF Magnetic Field Measurements Near the Epicenters of the Spitak (Ms = 6.9) and Loma Prieta (Ms=7.1) Earthquakes: Comparative Analysis, Geophys. Res. Letters, Vol. 19, No. 14, pages 1495-1498

Morrison, H. F.,Corwin, R.F., Fernandez, R.,1979, Earth resistivity, self potential variations, and earthquakes: A negative result for M=4.0: Geophysical Research Letters , vol. 6, no.3.

Mulgaria, F., Gasperini, P., 1992, Evaluating the statistical validity beyond chance of VAN earthquake precursors, Geophys. J. Int., 111, 32-44

Park S. K., Johnston M.J.S, Madden T.R., Morgan F.D., Morrison H.F., (1993), Electromagnetic Precursors to Earthquakes in the ULF Band: A review of Observations and Mechanisms, Reviews of Geophysics, Vol. 31, No. 2, pp117-132

Pulinets, S., Boyarchuk, K., 2004, Ionospheric Precursors of Earthquakes, Springer-Verlag, ISBN 3-540-20839-9

Simpson, F, Bahr, K, 2005, Practical Magnetotellurics, Cambridge University Press, ISBN 0-521-81727-7

Smith, J. T., (1995), Understanding Telluric Distortion Matrices, Geophysical journal International, v122, 219-226

Tullis, T. E., (1999), Deep Slip Rates on the San Andreas Fault, *Scienece vol. 285* no. 5428, pp. 671 - 672

Unsworth, M.; Egbert, G.; Booker, J. 1999: High-resolution electromagnetic imaging of the San Andreas fault in central California. Journal of Geophysical Research 104: 1131-1150

Uyeda S., Nagao T., Orihara Y., Yamaguchi T., Takahashi I. (2000), Geoelectric potential changes: Possible precursors to earthquakes in Japan, Proceedings of the National Academy of the Sciences, Vol 97, No. , pp4561-4566

Varotsos P., Alexopoulos K., 1984 Physical Properties of the Variations of the Electric Field of the Earth Preceding Earthquakes, I, Tectonophysics Vol 110, p73-98

Varotsos, P., Lazaridou, M.1991, Latest Aspects of Earthquake Prediction in Greece Based on Seismoelectric Signals, Tectonophysics, 188, p321-347

Varotsos, P., Alexopolous, K., Lazaridou, M., 1993, Latest Aspects of Earthquake Prediction in Greece Based on Seismoelectric Signals II, Tectono-

physics, 224, 1-37

Varotsos, P. ; Eftaxias, K. ; Vallianatos, F. ; Lazaridou, M. 1996 Basic principles for evaluating an earthquake prediction method Geophys. Res. Lett. Vol. 23 , No. 11 , p. 1295-1298 (96GL00905)

Wyss, M. 1996, Inaccuracies in seismicity and magnitude data used by Varotsos and coworkers, Geophys. Res. Lett. Vol. 23 , No. 11 , p. 1299-1302 (95GL03545)

Wyss, M., Allman, A. (1996) Probability of chance correlations of earthquakes with predictions in areas of heterogeneous seismicity rate: the VAN case, *Geophysical Research Letters v.23* No. 11, pp1307-1310

Zhao, Y., Qian, F., 1992, Geoelectric Precursors to Earthquakes in China, Proceedings of the Lake Arrowhead Workshop